



OPEN

Uncovering the molecular mechanisms of tonifying kidney and activating blood Decoction against myocardial fibrosis using network Pharmacology and experimental validation

Rui Xu^{1,6}, Yanping Bi^{1,6}, Yetao Ju², Wenhao Yin³, Shujun Zhao³, Yan Zhang^{2,4✉} & Xin Zhao^{1,5✉}

Chronic heart failure(HF) has become a disease of global concern due to its high morbidity and mortality.This has highlighted the need for cardioprotective agents.The Tonifying Kidney and Activating Blood(KTBA) decoction has been approved for clinical treatment of chronic HF.Tanshinone IIA(Tan IIA), rooted from *Salvia miltiorrhiza* of KTBA, has been approved for treating cardiovascular conditions.However, the mechanism is still unclear.This study examined the impact of KTBA on cardiomyocyte fibrosis in a rat model of heart failure post-myocardial infarction, induced by ligation of the left anterior descending coronary artery, followed by exhaustive swimming and starvation. Additionally, the effects of Tan IIA on CCD-841CoN cells were assessed under ischemic conditions in a 37 °C incubator with hypoxic environment (1% O₂, 5% CO₂, and 94% N₂). The investigation employed an integrative approach combining network pharmacology with molecular mechanism analysis.The findings of network pharmacology indicate that KTBA may exert its influence by targeting key proteins such as TNF, AKT1, STAT3, RELA (NF-κB p65), NFκBIA (I-κBα), and MAPK14 (p38α).Results showed that KTBA increased SERCA2a level, lowered collagen I and III, α-SMA, and phospholamban levels, reduced collagen fiber deposition, and delayed mitochondria injury.This cardioprotection effect was perhaps due to suppressing the expressions of p38MAPK, I-κBα, NF-κB, AQP4,AKT, PI3K, TNF-α, and STAT3 and increasing the levels of ZO-1 and Occludin in hippocampus of chronic HF rats, which were partially diminished by SB203580 and PDTC.Additionally, Tan IIA reduced levels of p38MAPK, I-κBα, NF-κB, STAT3, and increased levels of AQP4, Claudin-1, ZO-1, and ZO-2,that were reduced by siRNAs targeting p38MAPK, NF-κB, and AQP4.In conclusion, by modulating the p38MAPK/NF-κB/AQP4 axis, KTBA decoction delays cardiomyocyte fibrosis through alleviating hippocampal blood-brain barrier and Tan IIA improves enterocyte barrier integrity.

Keywords Chronic heart failure, Cardiac fibrosis, Tonifying kidney and activating blood Decoction, P38MAPK/NF-κB/AQP4 pathway, Network Pharmacology

Abbreviations

α-SMA	Alpha smooth muscle actin
AKT	Protein kinase B
AQP4	Aquaporin-4
BP	Biological process
CC	Cellular components

¹The Second Hospital of Dalian Medical University, Dalian 116023, China. ²The Affiliated Hospital of Liaoning University of Traditional Chinese Medicine, Shenyang 110032, China. ³Liaoning University of Traditional Chinese Medicine, Shenyang 110847, Liaoning, China. ⁴No.33Beiling Street, Shenyang, Liaoning, China. ⁵No.467Zhongshan Road, Dalian, Liaoning, China. ⁶Rui Xu and Yanping Bi contributed equally. ✉email: yanzhang1016@126.com; zx81830@163.com

COL I	Collagen I
COL III	Collagen III
DAPI	4',6-diamidino-2-phenylindole, dihydrochloride
DL	Drug-likeness
DMEM	Dulbecco's modified eagle's medium
ECG	Electrocardiogram
ECL	Enhancedchemiluminescence
EF	Ejection fraction
GO	Gene ontology
H&E	Hematoxylin and eosin
HF	Heart failure
HIF-1 α	Hypoxia-inducible factor-1 α
I- κ B α	Nuclear factor-kappa B inhibitor alpha
KEGG	Kyoto encyclopedia of genes and genomes
KTBA	Tonifying Kidney and Activating Blood
PDTc	Pyrrolidinedithiocarbamate ammonium
SB203580	4-(4-fluorophenyl)-2-(4-methylsulfinylphenyl)-5-(4pyridyl)-imidazole
LSD	Least-significant difference
MAPK	Mitogen-activated protein kinase
MF	Molecular functions
NF- κ B	Nuclear factor kappa-B
OB	Oral bioavailability
OD	Optical density
PDTc	Pyrrolidine dithiocarbamate
PI3 K	Phosphoinositide 3-kinase
PLN	Phospholamban
PPI	Protein-protein interaction
PVDF	Polyvinylidene fluoride
RT-qPCR	Reverse transcription quantitative real-time polymerase chain reaction
SB203580	4-(4-fluorophenyl)-2-(4-methylsulfinylphenyl)-5-(4-pyridyl)-imidazole
SERCA2a	Sarco(endo)plasmic reticulum Ca ²⁺ -ATPase 2a
siRNA	Small interfering ribonucleic acid
STAT3	Signal transducer and activator of transcription 3
Tan IIA	Tanshinone IIA
Tan IIA-H	Tanshinone IIA high dose
Tan IIA-L	Tanshinone IIA low dose
Tan IIA-M	Tanshinone IIA medium dose
TCM	Traditional Chinese medicine
TCMSP	Traditional chinese medicine systems pharmacology database and analysis platform
TNF- α	Tumor necrosis factor- α
UCG	Ultrasonic cardiogram
ZO-1	Zonula occludens 1
ZO-2	Zonula occludens 2

Chronic heart failure(HF) constitutes a multifaceted clinical syndrome, precipitated by pathological ventricular remodelling, compromised cardiac filling and ejection functionality, diminished cardiac output, and the incapacity to fulfil metabolic requirements¹. It represents the terminal phase of cardiovascular and other systemic diseases. This prevalent condition is associated with significant mortality and morbidity rates². In recent scholarly discourse within the cardiovascular domain, chronic HF has emerged as a challenging and compelling subject of study, with ventricular fibrosis identified as the primary pathological foundation for its onset and progression³. Ischaemic heart disease persistently serves as the primary cause of chronic HF. Despite advanced cardiovascular diagnostic techniques, immediate revascularization and subsequent implementation of optimized novel treatment strategies, a significant number of patients still develop to end-stage HF⁴⁻⁶. Therefore, it is crucial to find new ways to improve the prognosis and long-term survival of patients with HF. It is important to note that gastrointestinal and cerebral blood flow constitute 15% and 12% of cardiac output in resting adults, respectively⁷. Chronic HF is likely associated with reduced blood flow in mesenteric and cerebral arteries^{8,9}, which can trigger inflammation in gut epithelial cells and neuroinflammation^{10,11} to impair the intestinal and blood-brain barrier, maybe resulting in neurodegenerative condition¹². Moreover, the resultant impairment in gut and brain may be responsible for both direct and indirect myocardial injury, potentially exacerbating HF. Consequently, the gut and brain are susceptible and primary target organs of HF^{13,14}. Thus, understanding the two-way interaction between chronic HF and the brain or gut is essential for discovering new treatment targets.

The MAPK/NF- κ B cascades are evolutionary conserved, intracellular signal transduction pathways that control various cellular developmental processes, including cell growth, proliferation, differentiation, motility, stress response, survival and apoptosis^{15,16}. Additionally, NF- κ B plays a crucial role in inflammation and immune response^{17,18}. Recent studies have shown that p38MAPK/NF- κ B signaling plays an important role in myocardial fibrosis¹⁹, and blocking p38MAPK and NF- κ B can reduce myocardial fibrosis, leading to lower levels of Collagen I, Collagen II, and α -SMA^{20,21}. AQP4, a key membrane protein, aids in the transport of small molecule substances and water across the membranes of gut and blood-brain barriers. This protein's levels decrease in intestinal edema and increase in central nervous system edema^{22,23}. A research has documented

myocardial edema and fibrosis, increased myocardial stiffness, and heart insufficiency in rats with chronic HF, which showed elevated AQP4 levels²⁴. Another research has found a link between p38MAPK/NF-κB activation and AQP4 expression in hypoglycemia-induced brain injuries²⁵. A barrier to fluids across epithelium and endothelium is created by tight junctions, which consist of transmembrane proteins claudin and occludin and ZO-1^{26,27}. Injury to the blood-brain barrier and subsequent brain edema following intracranial hemorrhage in mice have been observed to worsen myocardial fibrosis outcomes²⁸. Phosphorylation of the MAPK/NF-κB signaling pathway was downregulated in brain microvascular endothelial cells, and an increase in tight junction protein expression in the blood-brain barrier was noted when pretreated with MAPK and NF-κB inhibitors²⁹.

In recent years, numerous researches have corroborated the multi-channel, multi-level, and multi-target attributes of traditional Chinese herbs for treating diseases over thousands of years^{30–32}. Traditional Chinese herbs provide a new option for the treatment of diseases. Tonifying Kidney and Activating Blood (KTBA) decoction is formulated for treating chronic HF summarized through years of clinical practice based on “Heart-Kidney Coordination” theory^{33,34} and is a blend of certain proportions of various dried plant parts, including the dry roots and rhizomes of *Polygonatum sibiricum*(Huangjing) and *Panax notoginseng*(Sanqi), the dry roots of *Salvia miltiorrhiza*(Danshen), *Astragalus mongholicus*(Huangqi), and *Panax ginseng*(Renshen); the dry mature seed of *Cuscuta chinensis*(Tusizi); the dry flower of *Carthamus tinctorius*(Honghua); and the dry root, stem, and leaf of *Leonurus japonicus*(Yimucao). And that its mechanisms of action may be related to promoting blood circulation, regulating mitochondrial energy metabolism, reducing inflammation, and adjusting endoplasmic reticulum stress^{35,36}.

The polysaccharides derived from *Polygonatum sibiricum* manifest their effects by mitigating the inflammatory response, hippocampal damage, and myocardial fibrosis via the modulation of the ERK1/2-NF-κB and JAK/STAT pathways^{37,38}. In addition, Salvinolic acid A has been discovered to reduce heart collagen levels and alleviate myocardial fibrosis mainly by reducing inflammatory cytokines and mediators via MAPK and NF-κB pathways³⁹. *Cuscuta chinensis* extract slows liver fibrosis by reducing α-SMA and Col1α1 mRNA levels⁴⁰. Extracts of *Astragalus mongholicus* effectively reduce fibrosis by inhibiting p38MAPK/NF-κB signaling and the deposition of Collagen I, Collagen III, and α-SMA^{41,42}. *Panax notoginseng* administration has been observed to reduce myocardial fibrogenesis by lowering Collagen1α1 and Collagen3α1 expressions⁴³ and downregulating MAPK and NF-κB expressions⁴⁴. This treatment also increases colonic TJP expression and decreases AQP4 protein levels, suggesting potential anti-neuronal edema effects^{45,46}. Ginsenoside Rg3 prevents Ang II-induced myocardial fibrosis via attenuating MyHc, Collagen I, and TGF-β1 by modulating the SIRT1/NF-κB pathway⁴⁷. Hydroxysafflor yellow A has been discovered to suppress the overexpression of α-SMA and Collagen I in human fetal lung fibroblasts and mice with pulmonary fibrosis^{48,49}. Leonurine significantly alleviates cardiac fibrosis and inflammation by inhibiting the MAPK and NF-κB pathways, offering a potential treatment for hypertensive HF⁵⁰. In summary, KTBA decoction shows a great anti-fibrosis effect.

Earlier researchs have shown that the KTBA decoction can influence AQP4 expression in heart, brain, and colon tissues, along with NF-κB and Occludin levels in heart and colon tissues^{51–53}. In this study, we established a rat model of HF following myocardial infarction via left anterior descending artery ligation, and exhaustive swimming and starvation to explore the protective effect of KTBA decoction on chronic HF via hippocampal p38MAPK/NF-κB/AQP4 pathways, utilizing the principles of “Kidney Storing Essence, Producing Marrow and Connecting to Brain”(Fig. 1).

Related works

Kidney stores essence, produces marrow and connects to brain in chronic HF

The brain is the house of spirit and the meeting of all yang, while the heart dominates spirit. During embryonic development, the brain marrow forms the five viscera consciousness, with the primordial spirit evolving into the heart spirit and then into five spirits⁵⁴. Visceral manifestation theory links brain physiology and pathology to the heart, dividing it into five viscera⁵⁵. The spirits reside in the brain but operate through the heart, highlighting

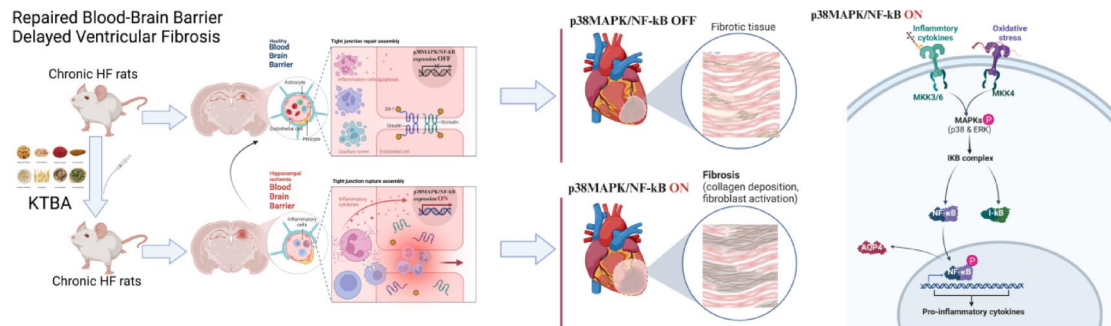


Fig. 1. Tonifying Kidney and Activating Blood decoction demonstrates potential therapeutic effects by inhibiting ventricular fibrosis and the activation of the p38MAPK/NF-κB signaling pathway, as well as repairing the blood-brain barrier in chronic heart failure rats. This suggests a significant role of the p38MAPK/NF-κB signaling pathway in the pathogenesis of ventricular fibrosis and blood-brain barrier damage. Abbreviations: MAPK, mitogen-activated protein kinase; NF-κB, nuclear factor kappa-B.(By BioRender (app.biorender.com)).

their close connection. The brain's role as the primary spirit relies on brain marrow enriched by heart blood and kidney essence. Together, they govern the spirits. The ancient medical text "Records of Traditional Chinese and Western Medicine in Combination" describes the brain as a sea of marrow, formed by true *yin* and *yang qi* from the kidneys, infused by the *Yuan qi* and *Du* meridians⁵⁶. Chi nan demonstrated the correlation between chronic HF and the "heart-brain-kidney" axis, thus, the treatment concept of "harmonization of heart, brain and kidney" is proposed in order to provide new ideas for the clinical treatment of chronic HF⁵⁷. However, there is a lack of extensive experimental evidence. The kidneys have the physiological function of "storing essence, generating marrow, and connecting to the brain". In this study, we propose the pathological essence of "Kidney storing essence, generating marrow, and connecting to the brain" "Brain storing mind, and heart storing spirit" and the hippocampal blood-brain barrier in chronic HF. It is that the kidney essence is abundant, the kidney generates marrow and connects to the brain, maintaining the integrity of the blood-brain barrier, delaying myocardial fibrosis, revealing the scientific connotation of "heart-brain-kidney".

KTBA restores hippocampal blood-brain barrier integrity by AQP4 and tight junctions in chronic HF

Chronic HF has been shown to compromise the integrity of the blood-brain barrier, potentially leading to neurodegenerative conditions¹¹. Damage to the blood-brain barrier and subsequent cerebral edema following intracranial hemorrhage in murine models have been associated with exacerbated myocardial fibrosis outcomes²⁸. In earlier research, our team demonstrated that KTBA can modulate disturbances in gut, cardiovascular, and cerebrovascular fluid metabolism, delay ventricular remodeling, and enhance cardiac function. This is achieved by downregulating the expression of AVP, AQP1, and AQP4 in brain tissue, as well as AQP1, AQP4, and AQP7 in myocardial tissue, while upregulating AQP4 and TJs in colon tissues in a rat model of HF post-myocardial infarction^{51–53}. In the current study, we further investigate the effects of KTBA decoction on the integrity of the hippocampal blood-brain barrier, focusing on the roles of AQP4 and tight junctions in chronic HF models.

KTBA regulates hippocampal AQP4 and TJs by inhibiting p38MAPK/NF-κB pathway in chronic HF

Li et al. demonstrated that the activation of the p38MAPK/NF-κB pathway affects the expression of AQP4 and tight junction proteins (TJs) in brain injuries induced by hypoglycemia²⁵. Zhu et al. observed that the phosphorylation of the MAPK/NF-κB signaling pathway is initiated in brain microvascular endothelial cells, leading to an increase in tight junction protein expression within the blood-brain barrier when pretreated with MAPK and NF-κB inhibitors²⁹. Liu et al. reported that bloodletting puncture at the twelve Jing-well points on the hand may significantly protect the blood-brain barrier by modulating the expression of MMP9 and AQP4, as well as the associated upstream ERK and p38 signaling pathways⁵⁸. The findings of Cai et al. suggested that a 3-day pre- and post-treatment with tongxinluo could serve as an effective therapeutic approach for brain ischemia by mitigating brain edema through AQP4 inhibition and reducing post-ischemic inflammation via NF-κB⁵⁹. In this study, pharmacological inhibitors were employed to demonstrate that KTBA can modulate hippocampal p38MAPK/NF-κB activity, thereby influencing blood-brain barrier function and establishing its upstream-downstream relationship in chronic HF.

KTBA delays myocardial fibrosis by hippocampal p38MAPK/NF-κB/AQP4 & TJs to exert a protective effect on heart in chronic HF

Studies have demonstrated that KTBA decoction exhibits significant clinical efficacy in the treatment of chronic HF^{33,34,60}. The anti-fibrotic effects of KTBA decoction, particularly through the Wnt pathway and the gut p38MAPK/NF-κB/AQP4 pathway^{61,62}, have garnered substantial scholarly interest. In alignment with the treatment concept of "harmonization of heart and brain", we investigate whether KTBA modulates hippocampal AQP4 and tight junction proteins, such as ZO-1 and Occludin, via the p38MAPK/NF-κB pathway to enhance hippocampal capillary permeability, restore blood-brain barrier function, and ultimately treat HF. However, it is important to note that this study represents only a portion of the drug's efficacy, suggesting that there may be additional mechanisms through which KTBA could be effective in treating chronic HF.

Results

Screening of KTBA-active compositions

In TCMSP, we discerned 144 active constituents within the KTBA on OB and DL. These constituents include 12 from *Polygonatum sibiricum*, 65 from *Salvia miltiorrhiza*, 11 from *Cuscuta chinensis*, 20 from *Astragalus mongolicus*, 22 from *Panax ginseng*, 22 from *Carthamus tinctorius*, 8 from *Leonurus japonicus*, and 8 from *Panax notoginseng*. Among these, 13 components are shared across the different medicinal herbs. Furthermore, five representative components can be identified from each of the eight selected medicinal herbs in Table 1.

Analysis of KTBA targets and chronic HF targets

Through the utilization of Swiss Target Prediction and Pharmapedia databases, 285 targets were identified for KTBA. Concurrently, a total of 12,528 targets were discovered for chronic HF through the GeneCards and DisGeNET disease target databases. These targets were subsequently integrated into Venny 2.1.0, yielding 276 common targets as depicted in Fig. 2A.

The PPI network of KTBA and chronic HF common targets

A PPI network was constructed utilizing 276 shared targets derived from the STRING database. This network exhibited an average degree value of 45. By employing CytoNCA in Cytoscape 3.9.1, a total of 108 core targets were identified, each with a degree value exceeding 45. Nodes with darker colors in the network represent higher

Molecule Name	Mol ID	CAS	MW	OB/%	DL	Chinese medicinal materials
3'-Methoxydaidzein	MOL002959	21913-98-4	284.28	48.56	0.24	<i>Polygonatum sibiricum</i>
Sitosterol	MOL000359	68555-08-8	414.79	36.91	0.75	<i>Polygonatum sibiricum</i>
Diosgenin	MOL000546	512-04-9	414.69	80.87	0.8	<i>Polygonatum sibiricum</i>
Baicalein	MOL002714	27462-75-5	270.25	33.51	0.2	<i>Polygonatum sibiricum, Carthamus tinctorius</i>
Beta-sitosterol	MOL000358	83-46-5	414.79	36.91	0.75	<i>Polygonatum sibiricum, Cuscuta chinensis, Panax notoginseng, Panax ginseng, Carthamus tinctorius</i>
Tanshinone IIA	MOL007154	568-72-9	294.37	49.88	0.39	<i>Salvia miltiorrhiza</i>
Isotanshinone II	MOL007111	20958-15-0	294.37	49.91	0.39	<i>Salvia miltiorrhiza</i>
Danshenol A	MOL007082	189308-08-5	336.41	56.96	0.52	<i>Salvia miltiorrhiza</i>
Cryptotanshinone	MOL007088	35825-57-1	296.39	52.34	0.39	<i>Salvia miltiorrhiza</i>
Poriferast-5-en-3beta-ol	MOL001771	83-47-6	414.79	36.91	0.75	<i>Salvia miltiorrhiza, Carthamus tinctorius</i>
Isorhamnetin	MOL000354	480-19-3	316.28	49.6	0.3	<i>Cuscuta chinensis, Astragalus mongolicus, Leonurus japonicus</i>
Kaempferol	MOL000422	520-18-3	286.25	41.88	0.24	<i>Cuscuta chinensis, Astragalus mongolicus, Panax ginseng, Leonurus japonicus, Carthamus tinctorius</i>
Quercetin	MOL000098	117-39-5	302.25	46.43	0.27	<i>Cuscuta chinensis, Astragalus mongolicus, Leonurus japonicus, Panax notoginseng, Carthamus tinctorius</i>
Sesamin	MOL001558	607-80-7	354.38	56.54	0.82	<i>Cuscuta chinensis</i>
Stigmasterol	MOL000449	83-48-7	412.77	43.82	0.75	<i>Panax notoginseng, Panax ginseng, Carthamus tinctorius,</i>
Ginsenoside rh2	MOL005344	112246-15-8	622.98	36.31	0.55	<i>Panax notoginseng, Panax ginseng</i>
Ginsenoside f2	MOL007475	62025-49-4	785.14	36.43	0.25	<i>Panax notoginseng</i>
Ginsenoside-Rh4_qt	MOL005348	174721-08-5	458.8	31.11	0.77	<i>Panax ginseng</i>
Calycosin	MOL000417	20575-57-9	284.28	47.75	0.24	<i>Astragalus mongolicus</i>
Isoflavanone	MOL000398	4737-27-3	462.49	109.98	0.29	<i>Astragalus mongolicus</i>
Galeopsin	MOL001418	76475-16-6	376.54	61.01	0.37	<i>Leonurus japonicus</i>
Preleoheterin	MOL001421	151178-05-1	334.5	85.97	0.33	<i>Leonurus japonicus</i>

Table 1. Information of constituents from tonifying kidney and activating blood Decoction.

degree values, suggesting that TNF, AKT1, STAT3, RELA (NF- κ B p65), NF κ BIA (I- κ B α), and MAPK14 (p38 α) serve as pivotal targets of KTBA in the treatment of chronic HF via the regulation of immune inflammation, as depicted in Fig. 2B.

GO analysis and KEGG pathway enrichment analysis

The aforementioned 108 key targets encompass a total of 6,256 Biological Processes (BP), 604 Cellular Components (CC), and 1,204 Molecular Functions (MF). At BP level, these key targets predominantly partake in responses to xenobiotic stimuli, responses to inorganic substances, cellular responses to organic cyclic compounds, and processes within the circulatory system. At CC level, the key targets are primarily located in membrane rafts, dendrites, receptor complexes, and transcription regulator complexes. The MF analysis reveals that these key targets are chiefly involved in transcription factor binding and neurotransmitter receptor activity, protein kinase binding, protein domain specific binding, nuclear receptor activity, as depicted in Fig. 2C.

Additionally, the most prominent 20 pathways of the enrichment of 296 KEGG pathways, which include Pathways in Cancer, Lipid and Atherosclerosis, TNF signaling pathway, and PI3 K-Akt signaling pathway, are illustrated in Fig. 2C.

A “Compounds-Targets-Pathways” network

The top 20 pathways, identified via KEGG analysis, with enriched targets were chosen for subsequent analysis. These targets, in conjunction with the corresponding compounds and pathways, were incorporated into the Cytoscape 3.9.1 software to establish a “compound-target-pathway” network, as illustrated in Fig. 2D. The results shown that quercetin, luteolin, kaempferol, tanshinone iia, and baicalein emerged as the top five active ingredients based on degree value, suggesting that compounds such as Tanshinone IIA (Tan IIA) may potentially

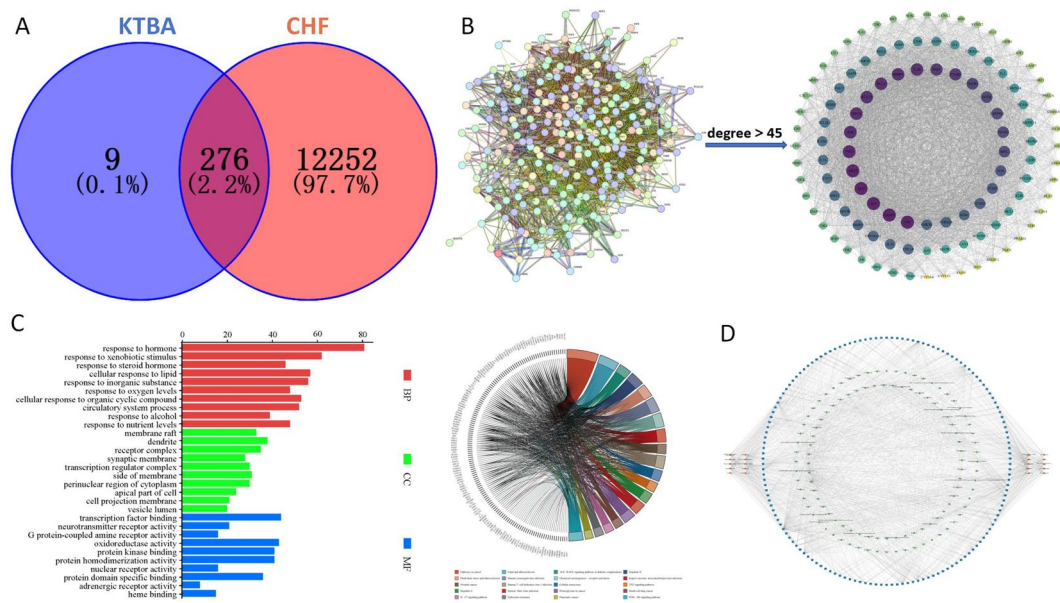


Fig. 2. The application of network pharmacology is utilized for the analysis of Tonifying Kidney and Activating Blood decoction and chronic heart failure. This includes a Venn diagram illustrating the targets of active constituents of Tonifying Kidney and Activating Blood decoction and chronic heart failure-related targets (A), a PPI network diagram of core targets (B), and an enrichment analysis diagram of GO (left) and KEGG pathway (right) (C). The “Active ingredients-key targets-pathway” network is also presented (D). Abbreviations: GO, gene ontology; KEGG, kyoto encyclopedia of genes and genomes; PPI, protein-protein interaction.

be pivotal in the treatment of chronic HF within KTBA. Furthermore, Tan IIA may modulate I- κ B α /NF- κ B pathway by targeting I- κ B α and NF- κ B p65.

Additionally, signaling pathways such as Pathways in Cancer, Lipid and Atherosclerosis were found to have a substantial impact on the treatment of chronic HF by KTBA. The outcomes of this research illustrate the effectiveness of traditional Chinese medicine formulas in managing diseases via the regulation of “multiple components, targets, and pathways”.

Molecular docking verification

The binding assessment of Tan IIA with five core targets [I- κ B α , AKT1, STAT3, p38MAPK, and NF- κ B p65] and three non-core targets [AQP4, ZO-1, and Occludin] was conducted through molecular docking process, as illustrated in Fig. 3.

Tan IIA exhibited robust binding activity with I- κ B α and AKT1, primarily facilitated by van der Waals forces. Furthermore, Tan IIA demonstrated significant binding activity with p65 NF- κ B, with the predominant interaction form being Pi-Cation and Pi-Anion between components and targets. Moreover, the hydroxyl groups present in the structure of Tan IIA established conventional hydrogen bonds with specific amino acid residues, including Met149 in AQP4, Ser508 in Occludin, and Tyr640 in STAT3. Concurrently, carbon hydrogen bonds were formed with amino acid residues such as Met175 in p38MAPK and Gln261 in ZO-1. A detailed account of the comprehensive docking scores is provided in Table 2.

KTBA exerts a protective effect on heart in chronic HF

Compared with the model group, both KTBA and tolvaptan significantly augmented the 24-hour urinary output (a marker for assessing fluid metabolism) in chronic HF rats ($p < 0.05$, Fig. 4C). Additionally, a reduction of the amount of deposited interstitium collagen fibers in the has been observed in both KTBA and tolvaptan groups (Fig. 4A-B). A consistent observation was that the quantities of type I and type III collagen fibers, along with α -SMA (all of which are critical mediators in myocardial repair), in the cardiomyocytes of the model group, were significantly higher than those in both KTBA-treated and tolvaptan-treated rats (Fig. 4D-E). In line with these findings, KTBA appeared to mitigate myocardial injury associated with HF (Fig. 4A-B). Histological examination revealed that the myocardial fibers of rats in the KTBA and tolvaptan groups exhibited a relatively regular arrangement. However, partial myocardial fibers in the infarction area were found to be broken and necrotic, with occasional instances of nucleus pyknosis or fragmentation. Furthermore, there was no significant hypertrophy observed in the cardiomyocytes of marginal area of myocardial infarction.

In comparison to the model group, the nucleus was located at the cell's edge with collagen fibers in the interstitial space, a condition improved in both KTBA and tolvaptan groups. Heart TEM results showed chronic HF models had significant myocardial mitochondrial damage, indicated by irregular myofibrils and vacuolated or swollen mitochondria with disrupted cristae, potentially remediable by KTBA. Meanwhile, KTBA

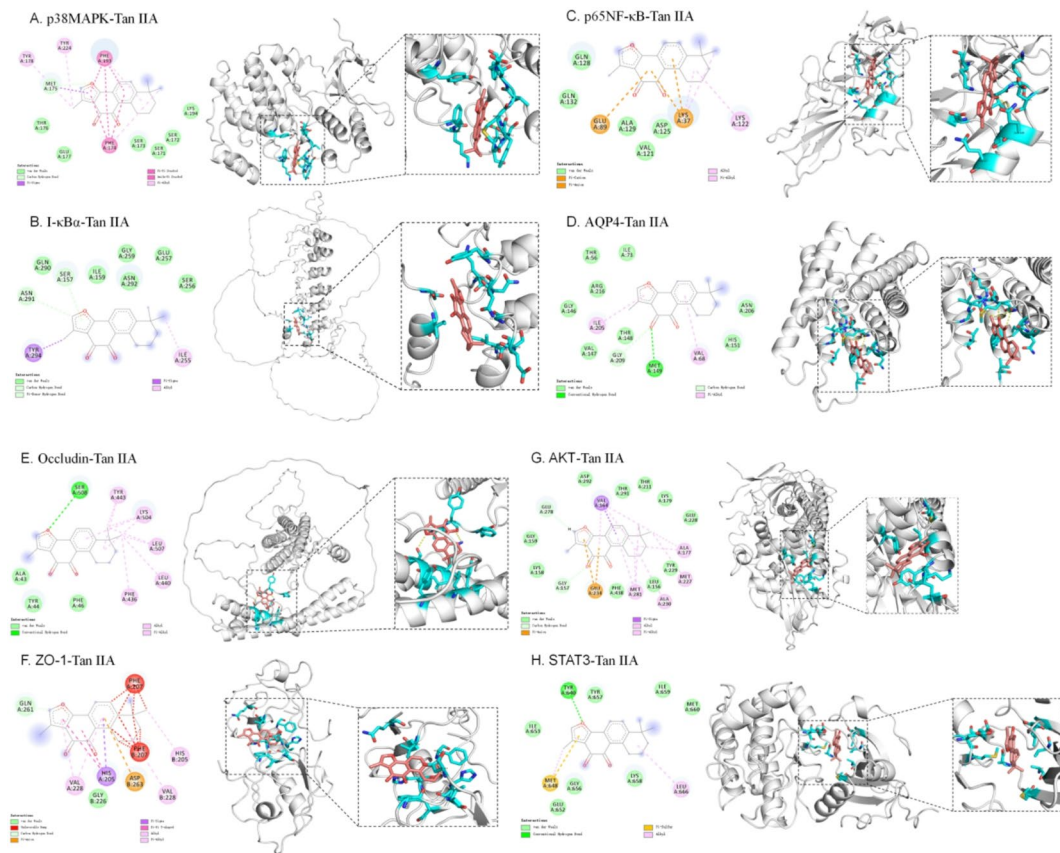


Fig. 3. Molecular docking technology is employed to examine the interaction between tanshininone IIA in the monarch drug *Salvia miltiorrhiza* of Tonifying Kidney and Activating Blood decoction and its targets. An analysis of the binding patterns of p38MAPK, I- κ B α , p65 NF- κ B, AQP4, Occludin, ZO-1, AKT, and STAT3 to tanshinone IIA is conducted, with the docking scores provided (A–H). Abbreviations: MAPK, mitogen-activated protein kinase; I- κ B α , nuclear factor- κ B inhibitor alpha; NF- κ B, nuclear factor kappa-B; AQP4, aquaporin-4; ZO-1, zonula occludens 1; AKT, protein kinase B; STAT3, signal transducer and activator of transcription 3.

Receptor	Binding Interaction Energy (kcal/mol)	VDW Interaction Energy (kcal/mol)	Electrostatic Interaction Energy (kcal/mol)
p38MAPK	-5.361	-28.786	-5.605
I- κ B α	-3.390	-21.848	-3.544
p65 NF- κ B	-3.560	-25.583	-3.722
AQP4	-5.260	-28.458	-5.499
Occludin	-4.292	-21.376	-4.487
ZO-1	-3.430	-24.518	-3.586
AKT1	-5.376	-32.867	-5.847
STAT3	-4.532	-23.190	-4.768

Table 2. Docking studies of Tanshinone IIA and key targets.

significantly augmented the protein expression of sarco(endo)plasmic reticulum Ca^{2+} -ATPase 2a (SERCA2a) while concurrently reducing the protein expression of phospholamban (a key regulator of SERCA2a-mediated myocardial relaxation during diastole) in chronic HF rats ($p < 0.05$, Fig. 4F–G).

These results suggest that KTBA decoction may improve fluid metabolism disorder, stabilize myocardial cell condition, maintain mitochondrial homeostasis, reduce the deposition of collagen in the myocardial interstitium, and alleviate myocardial fibrosis.

KTBA demonstrates a protective influence on hippocampus in the context of chronic HF

As depicted in Fig. 5A, KTBA mitigated varying levels of damage in the hippocampal CA1 region, characterized by the accumulation of chromatin at the edge, dissolution of the nuclear membrane, swelling of mitochondria,

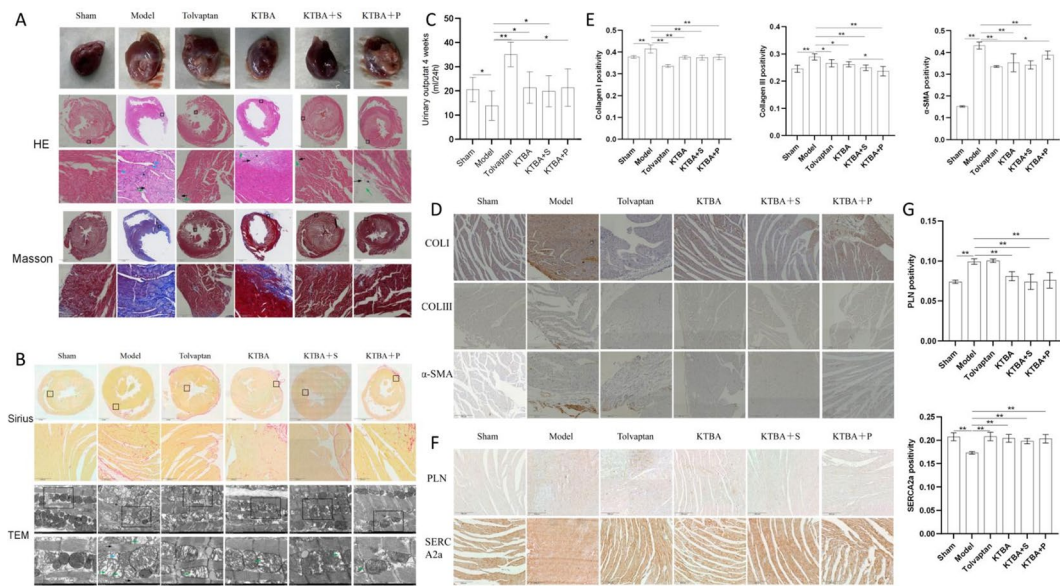


Fig. 4. Tonifying Kidney and Activating Blood decoction delays the onset of ventricular fibrosis in chronic heart failure. **(A)** Pathological and fibrosis images of heart, as demonstrated by Masson's trichrome staining (scale bar = 200 μ m) and hematoxylin and eosin staining (scale bar = 200 μ m). Pathological markers of myocardial hematoxylin and eosin staining include the following: a black arrow (\rightarrow) indicating the area of myocardial infarction; an asterisk (*) denoting significant infiltration of lymphocytes and neutrophils; a blue arrow (\rightarrow) pointing to swollen cardiomyocyte in the marginal area of myocardial infarction; and a green arrow (\leftarrow) highlighting dense fibrous connective tissue, which contains collagen fiber. **(B)** Representative images of fibrosis and mitochondrial structures in myocardial tissues, as visualized by Sirius Red staining (scale bar = 200 μ m) and transmission electron microscopy (scale bar = 1.0 μ m). The ultrastructural markers of myocardial tissue observed through transmission electron microscopy are as follows: the black arrow (\rightarrow) indicating an inordinance myofibrils; the blue arrow (\rightarrow) denoting mitochondria vacuolization; and the green arrow (\leftarrow) signifying mitochondria swelling with disrupted cristae and a blank zone. **(C)** Histogram of the 24-hour urinary output for six groups of rats at 4 weeks, $n = 8\text{--}9$. **(D-E)** The expression of α -SMA, COL I, and COL III proteins in the cardiac tissues, as determined by immunohistochemistry, $n = 3$. **(F-G)** The expression of PLN and SERCA2a proteins in the cardiac tissues, as examined using immunohistochemistry, $n = 3$. Note: * $p < 0.05$, ** $p < 0.01$. α -SMA, alpha smooth muscle actin; COL I, collagen I; COL III, collagen III; KTBA, Tonifying Kidney and Activating Blood; P, PDTC, pyrrolidine dithiocarbamate; S, SB203580; PLN, phospholamban; SERCA2a, sarco(endo)plasmic reticulum Ca^{2+} -ATPase 2a.

vacuolar degeneration of mitochondria, reduced density of pyramidal neurons, and disruption of tight junctions in the blood-brain barrier. This is evidenced by the increased expressions of tight junction proteins, specifically Occludin and ZO-1, which are integral components of tight junctions and serve as indicators of barrier integrity at the endothelial cell-cell contact regions within the hippocampus. The elevated expressions were observed in both KTBA-treated and tolvaptan-treated rats ($p < 0.05$, Fig. 5D-F). These observations suggest that both KTBA and tolvaptan may play a role in mitigating hippocampal injury.

KTBA inhibits hippocampal p38MAPK/NF- κ B/AQP4 signaling in chronic HF

There may be a correlation between neuroinflammation and chronic HF. Our findings support this association, as we observed that, in comparison to the model group, both KTBA and tolvaptan inhibited the protein expressions of p-p38MAPK/p38MAPK, p-I- κ B α /I- κ B α , p-p65 NF- κ B, p65 NF- κ B, PI3 K, AKT, STAT3, and TNF- α in hippocampal tissues (Fig. 5B, C). Additionally, p38MAPK, p65 NF- κ B, and I- κ B α mRNA were also suppressed (Fig. 5F). Furthermore, there was a significant decrease in the hippocampal AQP4 level, a hippocampal membrane integrin for transporting water molecules (Fig. 5B-F). This was observed following the administration of KTBA and tolvaptan.

Then, we implemented target gene silencing experiments using MAPK and NF- κ B inhibitors. Compared with the KTBA group, the combined KTBA plus SB203580 treatment led to the downregulation of p-p38MAPK, p-p65 NF- κ B, p65 NF- κ B, p-I- κ B α , PI3 K, AKT, STAT3, TNF- α , and AQP4 proteins in hippocampal tissues (Fig. 5B, C). Additionally, the combined treatment resulted in a decrease in p38MAPK, p65 NF- κ B, I- κ B α , and AQP4 mRNA levels (Fig. 5F). Similarly, the KTBA plus PDTC treatment led to the decrease in p-p65 NF- κ B, p65 NF- κ B, STAT3, and AQP4 proteins, while increasing the expressions of Occludin and ZO-1 in hippocampal tissues (Fig. 5D, E). Furthermore, this treatment reduced the level of I- κ B α mRNA and increased the levels of AQP4, Occludin, and ZO-1 mRNA (Fig. 5F). The findings collectively indicate that the treatment of chronic HF in rats with KTBA involves a longitudinal regulation of water metabolism via p38MAPK/NF- κ B/AQP4

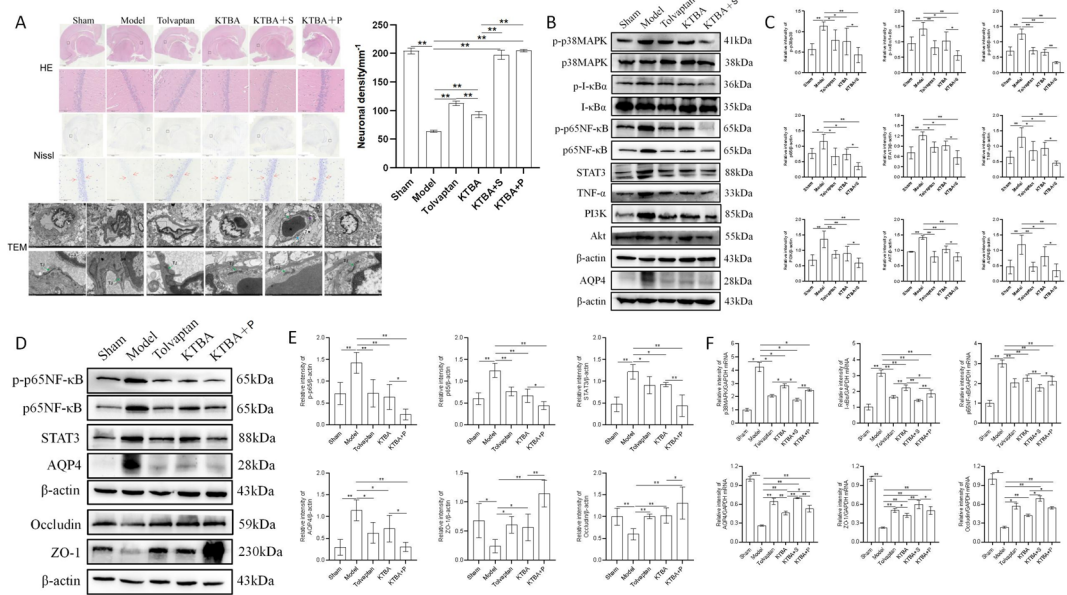


Fig. 5. Tonifying Kidney and Activating Blood decoction mitigates the disruption of the blood-brain barrier induced by chronic heart failure and to inhibit the expression of hippocampal p38MAPK/NF-κB pathway. (A) Pathological and intercellular junctions images, as captured using transmission electron microscopy (scale bar = 1.0 μm), hematoxylin and eosin staining (scale bar = 100 μm), and Nissl staining (scale bar = 100 μm). The blue arrow (“ \rightarrow ”) indicates capillary pericytes; the black arrow (“ \rightarrow ”) points to astrocyte foot board; the purple arrow (“ \rightarrow ”) identifies capillary endothelial cells; the asterisk (“ $*$ ”) highlights erythrocytes; the red arrow (“ $\rightarrow\leftarrow$ ”) denotes density change of pyramidal neurons in hippocampal CA1 region; the green arrow (“ \rightarrow ”) indicates intercellular tight junction change in hippocampal blood-brain barrier and its disruption in model rats. (B-C) The expression levels of proteins, including (p-)p38MAPK, (p-)p65 NF-κB, AQP4, (p-)I-κBa, STAT3, TNF- α , PI3 K, and AKT in hippocampal tissues of five groups of rats (including KTBA + S group) using western blot, $n = 3-4$. (D-E) The levels of (p-)p65 NF-κB, STAT3, AQP4, Occludin, and ZO-1 were examined in hippocampal tissues from the five groups of rats (including KTBA + P group) using western blot, $n = 3-5$. (F) The expression of p38MAPK, I-κBa, p65 NF-κB, AQP4, Occludin, and ZO-1 mRNA in hippocampal tissues using reverse transcription quantitative real-time polymerase chain reaction, $>n = 3$. Note: * $p < 0.05$, ** $p < 0.01$. AQP4, aquaporin-4; I-κBa, nuclear factor kappa-B inhibitor alpha; KTBA, Tonifying Kidney and Activating Blood decoction; P, PDTC, pyrrolidine dithiocarbamate; S, SB203580; MAPK, mitogen-activated protein kinase; mRNA, messenger ribonucleic acid; NF-κB, nuclear factor kappa-B; PI3 K, phosphoinositide 3-kinase; STAT3, signal transducer and activator of transcription 3; TNF- α , tumor necrosis factor alpha; ZO-1, zonula occludens protein 1.

signaling. This also encompasses an inherent mechanism of NF-κB intervention in tight junction proteins, which modifies the permeability of the hippocampal barrier and sustains its functionality.

HIF-1 α increases at 24 h of ischemia/hypoxia

We examined four hypoxia durations (36 h, 24 h, 12 h, and 6 h) and measured HIF-1 α levels. As depicted in Figure S2, there was a significant elevation in the HIF-1 α level at 24 h of ischemia/hypoxia-induced CCD-841 CoN cell in comparison to 24 h of normal cell (all $p < 0.05$). Consequently, 24-hour was chosen as the model time point for subsequent experiments.

Tan IIA influences cell viability in both normoxia and hypoxia

Upon administering varying concentrations (1.25, 2.5, 5, 10, and 20 $\mu\text{mol/L}$) of Tan IIA to CCD-841 CoN cells under diverse conditions (normoxia and hypoxia) and distinct time intervals (24 and 48 h), a significant inhibition of cell viability was observed after 48 h ($p < 0.05$). This inhibition demonstrated a dose-dependent relationship, reaching its peak at 1.25 $\mu\text{mol/L}$. Furthermore, under these varying concentrations and conditions, an increase in the treatment duration of Tan IIA correspondingly led to an increase in cell viability, which reached its zenith at 48 h. Based on the outcomes of the experiment, we selected three specific concentrations including a medium dose of 5 $\mu\text{mol/L}$, which demonstrated a cell viability rate of approximately 60%, a low dose of 2.5 $\mu\text{mol/L}$, and a high dose of 10 $\mu\text{mol/L}$, as well as a treatment time of 48 h for subsequent experiments, as illustrated in Figure S3, Table 3.

Transfection efficiency of CCD-841 CoN cells was higher at a ratio of 1.5 $\mu\text{L}/100\text{pmol}$

Efficiency was categorized into three groups based on different HG-TransGene™ to siRNA ratios. Group A utilized a ratio of 1.5 $\mu\text{L}/100\text{pmol}$, Group B employed a ratio of 1.2 $\mu\text{L}/80\text{pmol}$, and Group C incorporated a ratio of

Time Concentration	24 h (Normoxia24 h)	24 h (Hypoxia24 h)	48 h (Normoxia24 h)	48 h (Hypoxia24 h)
20umol/l	0.218253968	0.11550919	0.48530716	0.393730864
10umol/l	0.340608466	0.166510635	0.406500112	0.399607444
5umol/l	0.729497354	0.356543416	0.7738211	0.589127152
2.5umol/l	0.547619048	0.41383271	0.99287798	0.684621578
1.25umol/l	0.703703704	0.522822099	0.931435197	0.818313774

Table 3. CCD-841 CoN cell viability at different time and concentrations of Tanshinone IIA(mean).

1μL/60pmol. The data indicated that cells in Group A exhibited a higher siRNA transfection efficiency compared to the other groups. Future experiments consistently used the 1.5μL/100pmol ratio, as shown in **Figure S4**.

Tan IIA modulates inflammation, water metabolism and gut fluid barrier-associated proteins in ischemia/hypoxia-induced CCD-841 CoN cells

The interrelation between gut barrier dysfunction, water metabolism disorder, and inflammation in hypoxic conditions is well established. Our findings indicate that, in comparison to the control group, the model group exhibited elevated levels of p38MAPK, p65 NF-κB, I-κBa, STAT3, and Akt proteins, with the exception of PI3 K. Notably, these elevated levels were effectively suppressed by Tan IIA (all $p < 0.05$, Fig. 6A-B).

The Tan IIA-M group exhibited a lower concentration of p65 NF-κB and STAT3 proteins compared to both Tan IIA-L and furosemide groups (all $p < 0.05$, Fig. 6A-B). However, there was no significant difference observed in the inhibition of p38MAPK, I-κBa, and Akt protein expressions(all $p > 0.05$,Fig. 6A-B). Similarly, the Tan IIA-H treatment group displayed a lower concentration of STAT3 protein compared to the Tan IIA-L group ($p < 0.05$, Fig. 6A-B). These findings provide evidences that Tan IIA exerts an anti-inflammatory effect on p38MAPK, I-κBa, p65 NF-κB, STAT3, and Akt proteins, rather than on PI3 K. Furthermore, the chemoprotective effect of the Tan IIA-M group appears to be superior.The findings revealed that the optimal treatment range can be achieved when the dosage of Tan IIA reaches 2.5umol/L.

Compared to the control group, The levels of proteins related to water metabolism, such as AQP4, and gut fluid barrier-related proteins, including claudin-1, ZO-1, and ZO-2, were observed to be lower in the model group. However, these expressions were found to be reversed by Tan IIA and furosemide(all $p < 0.05$,Fig. 6A-B). The Tan IIA-H group exhibited a higher claudin-1 level compared to the Tan IIA-L group (all $p < 0.05$, Fig. 6A-B). Consistent with this, the Tan IIA-M group outperformed the Tan IIA-L group in up-regulating the expression of ZO-1 and ZO-2 proteins (all $p < 0.05$, Fig. 6A-B). These results suggest that Tan IIA may play a significant role in restoring gut fluid barrier function and ameliorating water metabolism disorder.

Tan IIA regulates p38MAPK/NF-κB/AQP4 signaling in ischemia/hypoxia-induced CCD-841 CoN cells

In Fig. 6C-E, the results revealed that the model group exhibited elevated expressions of p38MAPK and p65 NF-κB mRNA and positivity, coupled with reduced AQP4,Occludin and ZO-1 mRNA and positivity, compared to the control group.These trends were reversed following treatment with Tan IIA and furosemide.The group treated with Tan IIA-M exhibited lower levels of p38MAPK and I-κBa mRNA, and higher levels of AQP4,Occludin and ZO-1 mRNA, in comparison to both Tan IIA-L and Tan IIA-H groups.These findings suggest that Tan IIA may possess anti-inflammatory properties and potentially aid in rectifying dysbiosis in water metabolism and the restoration of gut fluid barrier function.Consistently, Tan IIA-M exhibited superior chemoprotective effects.

Additionally, there was no significant difference in the p38MAPK and I-κBa mRNA levels between the Tan IIA-M-treated and Tan IIA-M + p38 si groups(Fig. 6C-E). However, in comparison to the Tan IIA-M group, the Tan IIA-M + p38 si group exhibited lower p65 NF-κB and p38MAPK levels, and higher levels of AQP4, Occludin and ZO-1. Similarly, the Tan IIA-M + p65 si groups also showed a decrease in p65 NF-κB levels and an increase in AQP4, Occludin, and ZO-1 levels compared to the Tan IIA-M group. The latter alterations were reversed by the treatment of Tan IIA-M + AQP4 si.

In conclusion, our research suggests that Tan IIA enhances the expressions of AQP4 and TJP_s by inhibiting the p38MAPK/NF-κB pathway, indicating the chemopreventive effects of Tan IIA on CCD-841 CoN cells may be mediated via inflammation-water metabolism cascade signaling.

Discussion

The collection of network information and the efficiency of network interoperability are becoming increasingly important for research in fields such as medicine and security^{63,64}. In this investigation, we identified 144 active compounds and 276 direct target genes of KTBA.Through network pharmacology screening, we identified Tan IIA, a primary active ingredient of the monarch drug *salvia miltiorrhiza* Bunge in KTBA decoction. Furthermore, we identified 23 direct targets of Tan IIA, which has anti-inflammatory effect for cardiovascular diseases⁶⁵. In conclusion, our findings suggest that KTBA is a multi- component formula with a multi-target effect in the treatment of chronic HF.

The GO enrichment analysis revealed a correlation between KTBA and primary biological processes, including response to xenobiotic stimuli, response to inorganic substances, cellular response to organic cyclic compounds, and circulatory system processes. Furthermore, the KEGG pathway enrichment analysis indicated that KTBA could potentially have a therapeutic impact on chronic HF by modulating AKT1, TNF, STAT3,

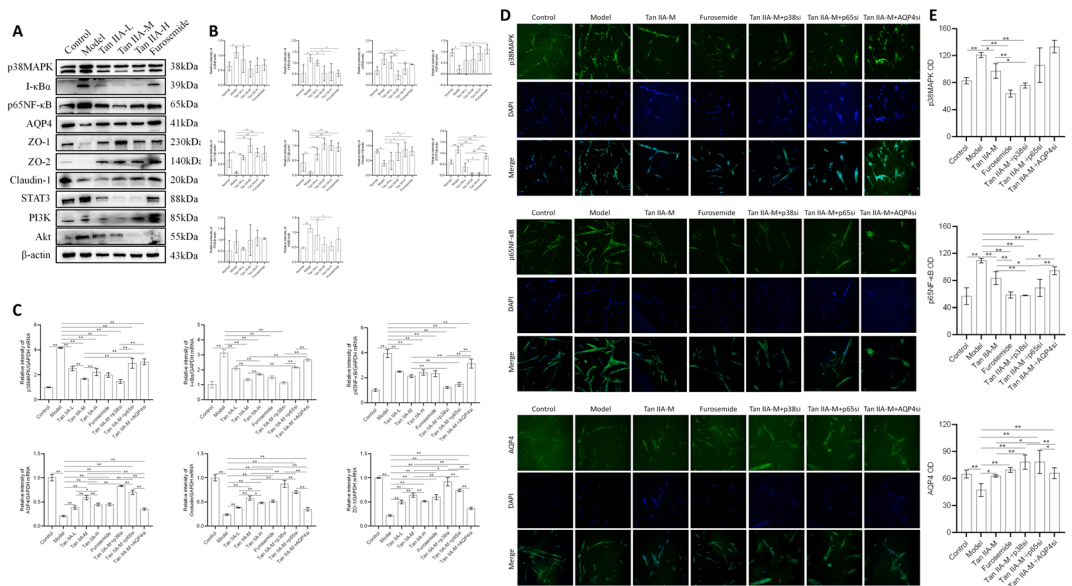


Fig. 6. Tanshinone IIA has been observed to regulate proteins associated with inflammation, water metabolism, and gut barrier in CCD-841 CoN cells subjected to ischemia/hypoxia. (A) Western blot analysis was conducted to examine The expression levels of inflammation proteins (PI3 K, AKT, p38MAPK, p65 NF- κ B, I- κ B α , and STAT3), water metabolism protein (AQP4), and gut barrier proteins (ZO-1, ZO-2, and Claudin-1) at 48 h across different experimental groups. (B) The relative expression intensities of the inflammation proteins p38MAPK, p65 NF- κ B, I- κ B α , STAT3, PI3 K and AKT, water metabolism protein AQP4, gut barrier proteins ZO-1, ZO-2, and Claudin-1 at 48 h using western blot, $n = 3$. (C) The relative intensity of p38MAPK, p65 NF- κ B, AQP4, I- κ B α , ZO-1, and Occludin mRNA at 48 h, as measured by RT-qPCR, $n = 3$. (D) Immunofluorescence images of p38MAPK, p65 NF- κ B, and AQP4 gene at 48 h. (E) The level of p38MAPK, p65 NF- κ B, and AQP4 proteins at 48 h, as quantified by immunofluorescence staining, $n = 3$. Note: * $p < 0.05$, ** $p < 0.01$. AKT, protein kinase B; AQP4, aquaporin-4; DAPI, 4',6-diamidino-2-phenylindole, dihydrochloride; I- κ B α , nuclear factor- κ B inhibitor alpha; mRNA, messenger ribonucleic acid; MAPK, mitogen-activated protein kinase; NF- κ B, nuclear factor kappa-B; PI3 K, phosphoinositide 3-kinase; RT-qPCR, reverse transcription quantitative real-time polymerase chain reaction; siRNA, small interfering ribonucleic acid; STAT3, signal transducer and activator of transcription 3; Tan IIA, tanshinone IIA; Tan IIA-H, tanshinone IIA high dose; Tan IIA-L, tanshinone IIA low dose; Tan IIA-M, tanshinone IIA medium dose; Tan IIA-M + AQP4 si, tanshinone IIA medium dose + aquaporin-4 small interfering ribonucleic acid; tan IIA-M + p38 si, tanshinone IIA medium dose + p38 small interfering ribonucleic acid; Tan IIA-M + p65 si, tanshinone IIA medium dose + p65 small interfering ribonucleic acid; ZO-1, zonula occludens 1; ZO-2, zonula occludens 2.

RELA (NF- κ B p65), NFKBIA (I- κ B α), and MAPK14 (p38 α). Additionally, Tan IIA may potentially affect the progression of chronic HF by targeting I- κ B α /NF- κ B pathway.

The molecular docking conformation, as revealed through computer simulation, indicated that Tan IIA successfully binds to the specific site of the protein targets such as I- κ B α and AKT by van der Waals forces, p65 NF- κ B by Pi-Cation and Pi-Anion, AQP4 by Met149, Occludin by Ser508, STAT3 by Tyr640, p38MAPK by Met175, ZO-1 by Gln261, which exhibit a substantial degree of three-dimensional conformational compatibility.

Myocardial infarction has been identified as a significant etiological factor in the progression of chronic HF²⁰. The onset of myocardial infarction leads to ischemic necrosis and apoptosis in the myocardial cells distal to the occluded vessel. The residual cardiomyocytes in the surrounding area respond with hypertrophy, while fibroblasts proliferate and subsequently transdifferentiate into myofibroblasts. This process results in the deposition of substantial quantities of extracellular matrix proteins, including collagen I and III, as well as α -SMA, that are crucial in myocardial repair. Nonetheless, excessive fibrosis diminishes ventricular compliance, instigating detrimental remodeling, and ultimately contributes to the development of chronic HF^{66,67}. In the present study, by establishing a rat model of chronic HF following acute myocardial infarction, we revealed swollen and irregular cardiomyocyte in the marginal area of myocardial infarction in chronic HF rats, and a significant deposition of collagen fibers in the interstitial zone with mitochondrial enlargement and myofibril rupture.

Researches have demonstrated that KTBA decoction has noteworthy clinical efficacy in the treatment of chronic HF with syndrome of *qi* deficiency and blood stasis^{33,34,60}. The anti-fibrotic effect and potential property to maintain mitochondrial homeostasis of KTBA decoction have attracted considerable scholarly attention^{61,62}. In this study, we have provided evidences that KTBA decoction exhibits a delaying effect on cardiomyocyte fibrosis and mitochondrial homeostasis imbalance. The extent of swollen myocardium in the marginal area of myocardial infarction and the deposition of collagen fibers within the interstitial zone were notably reduced. Additionally, KTBA decoction displayed significant improvements in irregular arrangement of myofibrils and

the condition of vacuolated or swollen mitochondria with broken crista. Collagen I, Collagen III, and α-SMA are implicated in the processes of myocardial fibrosis and myofibroblast activation⁶⁸. Through this study, we illustrated that KTBA decoction reduced of myocardial Collagen I and III, as well as α-SMA expression in chronic HF rats. Furthermore, phospholamban(PLN) plays a crucial role in regulating cardiac calcium transport and maintaining mitochondrial homeostasis. The regulation of intracellular Ca²⁺ is key to cardiac function. A large fraction of Ca²⁺ is released from the sarcoplasmic reticulum (SR) to initiate contraction and is pumped back into the SR to initiate relaxation by the sarco(endo)plasmic reticulum Ca²⁺-ATPase SERCA2a, the activity of which is regulated by PLN⁶⁹. In the present study, a decrease of PLN level and an increase of SERCA2a level were observed in rats treated with KTBA. Urinary output serves as an indicative marker for the assessment of dynamic shifts in capacity load experienced by patients suffering from HF⁷⁰. We observed that the 24-hour urinary output of chronic HF rats treated with KTBA decoction exhibited an increase. The results of this study suggest that KTBA decoction has the potential to decrease cardiac volume overload, preserve mitochondrial homeostasis, and mitigate myocardial fibrosis.

In recent years, the impact of changes in the mental state and characteristics of the brain on human functions has received increasing attention⁷¹. Additionally, previous studies have highlighted the neuroprotective properties of the KTBA decoction, a topic that has garnered increasing scholarly interest^{33,53}. Notably, we provided an inaugural evidence for the first time that KTBA decoction alleviates hippocampal injury in rats with chronic HF, which was linked to the p38MAPK/NF-κB/AQP4 pathway. KTBA mitigated varying levels of damage in hippocampal CA1 region, characterized by mitochondrial swelling, mitochondrial vacuolar degeneration, reduced density of pyramidal neurons, and disruption of the blood-brain barrier's tight junctions. The tight junction proteins, Occludin, ZO-1, and Claudin-1, are recognized markers of barrier integrity at the cell-cell contact regions of endothelial and epithelial cells in the hippocampus and gut⁷². Furthermore, myocardial fibrosis was found to be correlated with abnormal tight junction proteins in the brain²⁸, and the utilization of *qi*-tonifying and blood-activating herbs has been shown to mitigate the disruption of the blood-brain barrier^{73,74}. Tolvaptan is primarily utilized in the management of refractory HF, especially in patients who present with electrolyte disorder and diuretic resistance⁷⁵. Additionally, tolvaptan has been shown to mitigate cerebral edema by upregulating the expression of tight junction proteins ZO-1 and Occludin⁷⁶. In accordance with these findings, the elevated expression levels of Occludin and ZO-1 suggest that KTBA decoction potentially restores the function of hippocampal blood-brain barrier in chronic HF rats. Furthermore, no significant variance was observed between the therapeutic effects of KTBA and tolvaptan. In a related context, a significant upregulation of gut barrier-associated markers, including Claudin-1, Occludin, ZO-1, and ZO-2 proteins, was detected in Tan IIA-treated CCD-841 CoN cells. In summation, our findings propose that Tan IIA ameliorates the function of the gut fluid barrier by augmenting the expression of TJs, which may potentially aid in the rectification of fluid dysbiosis.

Previous studies indicated that both p38MAPK and NF-κB pathways play an important role in the development of organs and tissues^{77,78}. The p38MAPK and NF-κB signaling pathways in the brain have been associated with the pathophysiology of HF, playing a role in neuroinflammation and cardiomyocyte fibrosis^{79,80}. The inhibition of p38MAPK/NF-κB in neurocytes serves to mitigate the systemic inflammatory response and decrease injury ensuing from brain ischemia⁸⁰. Given that KTBA demonstrated the ability to restore blood-brain barrier function in chronic HF models, we investigated how KTBA alleviates chronic HF by examining signaling mechanisms through multiple sequence alignment, namely RNA and proteins⁸¹. KEGG analysis revealed that KTBA suppresses MAPK and NF-κB pathways. Ishikawa et al. found that tolvaptan can treat end-stage HF by inhibiting the phosphorylation of MAPK and NF-κB⁸². Our research provides the first empirical validation of significant reductions in the expression of p-p38MAPK, p-p65 NF-κB, and p-I-κBα in the hippocampal endotheliocytes of HF rats treated with KTBA and tolvaptan. This suggests that KTBA may inhibit the p38MAPK/NF-κB signaling pathway. Prior researchs have demonstrated that Tan IIA treatment can suppress multiple inflammatory-associated pathways in the intestinal region, including p38MAPK, NF-κB signaling, and Akt pathways. Furthermore, Tan IIA restored gut epithelial barrier by increasing the levels of ZO-1 and Occludin⁸³⁻⁸⁵. In this study, we observed that Tan IIA and furosemide significantly diminished the protein content of p38MAPK, I-κBα, p65 NF-κB, STAT3, and Akt. This suggests that p38MAPK and p65 NF-κB signaling are two primary pathways involved in ischemia/hypoxia CCD-841 CoN cell models. Importantly, the medium dose of Tan IIA, which exerted chemopreventive effect, was identified as the optimal dose and not inferior to furosemide.

AQP4, an integral membrane protein responsible for the mediation of water flux across the membrane of the blood-brain barrier and colonic epithelial cells, was found to increase in central nervous system edema and decrease in colon edema^{23,86}. Furthermore, the reduction of AQP4 expression in astrocyte and kidney was observed with the use of tolvaptan and furosemide^{87,88}. Our research demonstrated that both KTBA decoction and tolvaptan significantly mitigate brain edema by reducing AQP4 level in hippocampal tissue. These results suggest that KTBA decoction has a potential to inhibit neuroinflammation, alleviate cerebral edema, and restore blood-brain barrier integrity in chronic HF rats. Furthermore, our study also revealed that both Tan IIA and furosemide significantly enhance water homeostasis by increasing AQP4 level in ischemia/hypoxia-induced CCD-841 CoN cell models. Similarly, the medium dose of Tan IIA was be the most effective dosage and employed for subsequent transfection study.

Research indicated that p38MAPK initiates the phosphorylation of I-κB, leading to the depolymerization of I-κB and NF-κB. Subsequently, NF-κB undergoes nuclear translocation, and the activation of NF-κB (p65) is enhanced, regulating AQP4 gene, which may result in water metabolism disorder and barrier disruption⁸⁹. The p38MAPK inhibitor was observed to significantly decrease the levels of p-p38, p-p65, and AQP4 in the cortex and astrocytes of rats⁸⁹ and augment the expression of cerebral and intestinal TJs⁹⁰⁻⁹². Liu et al. discovered that the administration of SB203580 to C57BL/6 mice resulted in a relative inhibition of their activations, and

significantly downregulated brain AQP4 level⁹³. In the present study, we found that KTBA-plus-SB203580 decreased the phosphorylation of MAPK and NF-κB, and AQP4 level, and increase the expression of Occludin and ZO-1 in rat hippocampus. Furthermore, the application of siRNA to p38 was found to significantly impede NF-κB activity⁹⁴. Additionally, p38 siRNA transfection lessened the impact of 6-Gingerol on NF-κB in IEC-6 cells induced by hypoxia/reoxygenation⁹⁵. Consistent with these observations, Tan IIA-M plus p38 siRNA decreased NF-κB and MAPK levels and increased expression of AQP4, Occludin, and ZO-1 in CCD-841 CoN cells. These results propose that p38MAPK is located upstream of p65 NF-κB, AQP4, and TJs, possessing the ability to activate p65 NF-κB and regulate AQP4 while concurrently inhibiting the expression of TJs.

The NF-κB inhibitor suppressed the expression of p-p65 and AQP4, while simultaneously enhancing the expression of TJs in brain⁹¹. PDTC intervention reduced p-NF-κB and AQP4 levels of mouse astrocytes⁹⁶. SiRNA mediated p65 knock down significantly upregulated Claudins and ZO-1 expressions⁹⁷. Consistently, This study revealed that both KTBA-plus-PDTC and Tan IIA-M plus p65 siRNA inhibited p65 NF-κB expression, while concurrently regulate the expression of AQP4, Occludin, and ZO-1 in rat hippocampus and CCD-841 CoN cell, indicating p65 NF-κB being upstream of AQP4, ZO-1, and Occludin genes. The data further suggests that KTBA and Tan IIA modulate AQP4, ZO-1, and Occludin expressions via the p38MAPK/NF-κB pathway, thereby maintaining fluid metabolism and repairing barrier integrity.

Research findings suggest that the knockdown of AQP4 by siRNA in astrocytes significantly diminishes the degradation of tight junctions⁹⁸. Data derived from our study suggested that the treatment with Tan IIA-M + AQP4 siRNA leads to a reduction in the expression of AQP4, Occludin, and ZO-1 mRNA, highlighting the possible involvement of AQP4 in the regulation of TJs. Furthermore, Tan IIA appears to modulate ZO-1 and Occludin expressions via AQP4 signaling.

Taken together, our data showed that KTBA decoction delayed myocardial fibrosis in rats with chronic HF after myocardial infarction via hippocampal p38MAPK/NF-κB/AQP4 signaling pathway. Yet, there may be another way to treat chronic HF with KTBA, as this study is only part of the drug's efficacy.

Conclusions

Our research reveals the first activation of hippocampal p38MAPK/NF-κB/AQP4 pathway in the during chronic HF, linking it to blood-brain barrier damage and myocardial fibrosis. Additionally, we demonstrate that KTBA can chemoprevent chronic HF in vivo by restoring blood-brain barrier integrity and delaying cardiomyocyte fibrosis through modulation of the p38MAPK/NF-κB pathway. This understanding will inform future strategies for leveraging KTBA to prevent chronic HF. This study solely examined the impact of KTBA on hippocampal blood-brain barrier and p38MAPK/NF-κB/AQP4 signaling pathway in chronic HF rats by pharmacological inhibitors. Knockout of target gene or pharmacological agonist, and neuronal activity regulatory proteins and cognitive function related-Morris water maze were not conducted. Consequently, potential biases may exist in the results. As a result, our research team intends to conduct additional fundamental investigations on brain in animals using KTBA for chronic HF, with the aim of further verifying the pharmacological mechanisms and efficacy of this formulation.

Scientific contribution

Theoretical innovation: We propose the pathological essence of “Kidney storing essence, generating marrow, and connecting to the brain” “Brain hiding mind, heart dominating mind” and the hippocampal blood-brain barrier in chronic heart failure. It is that the kidney essence is abundant, the kidney generates marrow and connects to the brain, maintaining the integrity of the blood-brain barrier and maintaining stable barrier function, delaying myocardial fibrosis, revealing the scientific connotation of “heart-brain-kidney”.

Practical innovation: Clinical research has found that KTBA decoction has significant therapeutic effects on chronic heart failure. It is proposed that the kidney tonifying and blood activating formula regulates AQP4 and tight junction related proteins ZO-1 and Occludin through the p38MAPK/NF-κB pathway to improve hippocampal capillary permeability, restore blood-brain barrier function, delay myocardial fibrosis, and treat chronic heart failure.

In conclusion, the originality of scientific contributions to the state of the art are as follows:

- 1) Theory: Kidney stores essence, produces marrow and connects to brain.
- 2) KTBA restores hippocampal blood-brain barrier integrity by AQP4 and tight junctions.
- 3) KTBA regulates hippocampal AQP4 and TJs by inhibiting p38MAPK/NF-κB pathway.
- 4) KTBA delays myocardial fibrosis to exert a protective effect on heart.

In vivo(Fig. 7A)

Materials and methods

Creating a library for analyzing Kidney-Tonifying and Blood-Activating formula

In the Traditional Chinese Medicine Systems Pharmacology Database and Analysis Platform (TCMSP, <http://tcm-spw.com/>), eight traditional Chinese medicines were used as search terms. These include *Polygonatum sibiricum* Redouté (Asparagaceae), *Salvia miltiorrhiza* Bunge (Lamiaceae), *Cuscuta chinensis* Lam. (Convolvulaceae), *Astragalus mongolicus* Bunge (Fabaceae), *Panax ginseng* C.A.Mey. (Araliaceae), *Carthamus tinctorius* L. (Asteraceae), *Leonurus japonicus* Houtt. (Lamiaceae), and *Panax notoginseng* (Araliaceae). These plants are included in the Tonifying Kidney and Activating Blood Formula. The constituents were meticulously gathered and recorded, with the composition of the compound formula ascertained in accordance with references and the Pharmacopoeia of the People's Republic of China 2020 Edition. It is imperative that all ingredients satisfy certain prerequisites such as retrievability in the Traditional Chinese Medicine Systems Pharmacology (TCMSP)

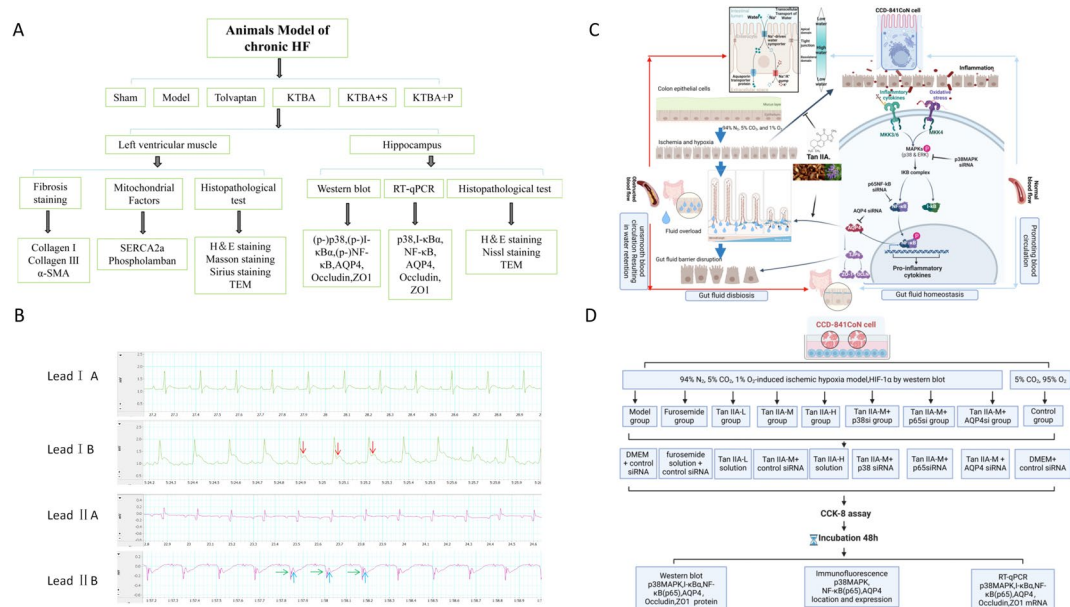


Fig. 7. (A) Technology Roadmap for Animal Experimentation In Vivo. (B) The ECG of rats were analyzed both before and after the ligation of the LAD artery. Figure Lead I A and Lead II A illustrates the ECG recorded prior to the surgical procedure, whereas Figure Lead I B and Lead II B displays the ECG obtained post-surgery. The red arrow (↓) indicates the elevation of the ST-segment, a hallmark of acute myocardial infarction, specifically anterior lateral infarction, implicating the LAD as the responsible vessel. The blue arrow (↑) denotes ST-segment depression and T wave inversion, while the green arrow (→) signifies the presence of a pathologic QS complex. (C) Tanshinone IIA was found to inhibit the dysregulation of water metabolism, disruption of the gut fluid barrier, and p38MAPK/NF-κB pathway. These processes are typically observed in hypoxia-induced CCD-841 CoN cells, with the p38MAPK/NF-κB signaling pathway playing a significant role in the dysbiosis of water metabolism and disruption of the gut fluid barrier. Therefore, the potential of Tanshinone IIA as an inhibitor of these processes warrants further investigation. (By app.biorender.com). (D) Technology Roadmap for Cell Experimentation In Vitro. Abbreviations: ECG, electrocardiogram; LAD, Left anterior descending; MAPK, mitogen-activated protein kinase; NF-κB, nuclear factor kappa-B.

database, compliance with the specifications of the 2020 edition of the Pharmacopoeia of the People's Republic of China, and substantiated active ingredients.

Identifying key elements and objectives

This study uses the ADME model to determine the Oral Bioavailability (OB) and Drug-likeness (DL) of drug components, leveraging the TCMSP database. Select active ingredients with an OB of at least 30% and a DL of 0.18 or more, along with their associated protein targets, from the KTBA compound analysis library. Import these selected active constituents into the SwissTargetPrediction and Pharmapper databases for the identification of potential drug targets. Consolidate the data and eliminate any duplicates to establish a comprehensive list of action targets for the active constituents of the KTBA compound. Use the search feature on the UniProtKB section of the UniProt website (<https://www.uniprot.org>) to obtain protein target identifiers and gene names relevant to the KTBA decoction. Employ Venny2.1.0 to generate Venn diagrams and identify overlapping targets.

Identifying targets for chronic heart failure

Search for 'Chronic Heart Failure' on the GeneCards website (<https://www.genecards.org/>) and keep targets with an Inference Score of at least 0.8. Likewise, conduct a search for 'Heart Failure' using the Gene Map Advanced Search feature on the OMIM website (<https://omim.org/>). Visit the DisGeNET database (<https://www.disgenet.org/search>) and navigate to the Disease section. Look up 'Chronic Heart Failure' and keep the targets labeled with 'M' (biomarkers or etiological factors) and 'T' (treatment targets) in the Direct Evidence part of the gene category. The identification of disease targets was achieved through the utilization of the GeneCards, OMIM, and DisGeNET databases. The data obtained from these databases are consolidated, and any duplicates are eliminated to isolate targets pertinent to chronic heart failure.

Building and analyzing protein-protein interaction networks

Subsequently, the active ingredient targets in the KTBA decoction were amalgamated with the targets related to heart failure in order to discern shared characteristics. The STRING database search tool was utilized to conduct a protein-protein interaction (PPI) network analysis on the common targets of the given disease and medication. The organism selected was Homo sapiens, with an established minimum interaction score threshold of medium confidence(0.900). Proteins not targeted were excluded from the analysis. Subsequently, the protein interaction

information was exported and the network was brought into Cytoscape 3.9.1 for visualization. The ‘Network Analyzer’ plugin was utilized to determine node degree values, serving as a metric to identify potential key targets of the KTBA compound in chronic heart failure treatment.

Identifying gene ontology for target locations and examining Kyoto encyclopedia of genes and genomes pathways
 Following this, an enrichment analysis was performed using the Metascape platform to elucidate the Gene Ontology (GO) and Kyoto Encyclopedia of Genes and Genomes (KEGG) pathways^{99–101} involved in KTBA’s anti-Chronic Heart Failure effects. Additionally, bioinformatics tools were employed to perform GO and KEGG enrichment analysis on the key genes, and the obtained findings were visually displayed.

Creating a network of the “Compounds-Targets-Pathways”

Irrelevant targets and components were eliminated from the drug. Network and type files were created, and Cytoscape 3.9.1 was utilized to establish connections between compounds, key targets, and pathways. This facilitated the construction of a network diagram and subsequent network’s topological parameters analysis.

Molecular docking

To validate the credibility of the interaction between tanshinone IIA, and core targets [NFKB1α(I-κBa), AKT1, STAT3, MAPK14(p38α), RELA(NF-κB p65)] as established in Sect. 1.6, a molecular docking procedure was executed. Targets related to the epithelial cell barrier (AQP4, ZO-1, Occludin) were incorporated into the docking validation process. Acquiring specific proteins from the RCSB PDB database (<https://www.rcsb.org/>) requires multiple stages. Initially, PDB format files are downloaded, followed by the removal of crystalline water and small molecules using the Pymol software. Afterward, chemical compounds are obtained from the PubChem database (<https://pubchem.ncbi.nlm.nih.gov/>) and subsequently transformed into the ‘*.mol2’ format via ChemDraw. The proteins and compounds are processed using AutoDockTools1.5.6, and then converted to pdbqt format for molecular docking with Vina1.5.6. The final step involves visualizing and analyzing the results with Pymol.

Animals

The study employed 91 male Sprague Dawley (SD) rats, free from specific pathogen, aged 13 weeks and weighing 180–220 g. The rats were obtained from Liaoning Changsheng Biotechnology Co., Ltd. Following the initial phase, the rats were adaptively fed for one week at the Animal Experiment Center of Liaoning University of Traditional Chinese Medicine. These rats were maintained in a controlled environment, featuring a related humidity level of 50% ± 5%, a temperature of 23 ± 3 °C, and 12 h/12 h brightness cycle. The diet of the rats consisted of standard forage procured from Shenyang Maohua Biotechnology Co., Ltd, and water was available to them at all times. The cleanliness of the environment was maintained by changing the cage pads every 2–3 days.

Drugs

- 1) Tolvaptan(15 mg) from Zhejiang Otsuka Pharmaceutical Co., Ltd (Lot No.:11107 S) was dissolved in double-distilled water to make a 0.135 mg/ml solution.
- 2) SB203580 from APExBIO Technology (Catalog No.: A8254) was dissolved in Dimethyl sulfoxide to prepare a 0.225 mg/ml solution.
- 3) PDTC from Beyotime Biotechnology (Catalog No.: S1809) was dissolved in Dimethyl sulfoxide to create an 18 mg/ml solution.
- 4) KTBA decoction, containing a blend of eight herbs, was obtained from the Affiliated Hospital of Liaoning University of Traditional Chinese Medicine. A standard decoction method was applied to preparing 20 g of dried *Polygonatum sibiricum* root and rhizome from the Asparagaceae family, 30 g of dried *Salvia miltiorrhiza* root from the Lamiaceae family, 20 g of dried *Cuscuta chinensis* mature seeds from the Convolvulaceae family, 40 g of dried *Astragalus mongolicus* root from the Fabaceae family, 10 g of dried *Panax ginseng* root from the Araliaceae family, 15 g of dried *Carthamus tinctorius* flowers from the Araliaceae family, 20 g of dried *Leonurus japonicus* root, stem, and leaves from the Lamiaceae family, and 5 g of dried *Panax notoginseng* root and rhizome from the Araliaceae family, aiming for a crude drug concentration of 1.575 g/ml. Plant names were verified via <http://mpns.kew.org/Medicinal>. Substances were stored at 4 °C. The information on plant ingredients of KTBA decoction is listed in **Table S1**.

Materials and equipment

The primary reagents and instruments utilized in this investigation are meticulously delineated in Table 4.

HPLC of KTBA

Instrument: Agilent 1290 Infinity II Ultra High Performance Liquid Chromatography (Agilent Technologies, USA).

Reagent: Acetonitrile (chromatographically pure, Merck, Germany); Formic acid (chromatographically pure, Tianjin Kemio Chemical Reagent Co., Ltd.); Water (purified water, Hangzhou Wahaha Group Co., Ltd.).

Preparation of test solution: Take each medicinal herb and add water according to the prescription to make KTBA decoction. Accurately measure 30 mL of the decoction, concentrate it, and make up to 10 mL. Accurately add 10 mL of anhydrous ethanol, let it stand, filter it, and take the continuous filtrate and filter it through a 0.22 μm microporous membrane to obtain it.

Chromatographic conditions: Column: Agilent Poroshell 120 EC-C18 (4.6 mm × 100 mm, 2.7 μm). The mobile phase was composed of 0.1% formic acid in water (Phase A) and acetonitrile (Phase B). The gradient for elution was set as follows: from 0 to 5 min, 5% B; from 5 to 7 min, 5% B to 8% B; from 7 to 16 min, 8% B; from 16 to 18 min, 8% B to 10% B; from 18 to 30 min, 10% B to 16% B; from 30 to 40 min, 16% B; from 40 to 55 min, 16% B

Reagents	Source	Identifier
AKT	Abcam	Cat#ab8805
p-AKT	Abcam	Cat#ab38449
AQP4	Abcam	Cat#ab259318
Claudin-1	Proteintech	Cat#28674-1-AP
Collagen I	Abcam	Cat#ab316222
Collagen III	Abcam	Cat#ab7778
HIF-1 α	Abcam	Cat#ab179483
I- κ B α	Abcam	Cat#ab32518
p-I- κ B α	Abcam	Cat#ab133462
Occludin	Abcam	Cat#ab216327
p38MAPK	Abcam	Cat#ab170099
p-p38MAPK	Abcam	Cat#ab4822
NF- κ B	Cell Signaling Technology	Cat#8242
p-NF- κ B	Cell Signaling Technology	Cat#3033
phospholamban	Cell Signaling Technology	Cat#14,562
PI3 K	Abcam	Cat#ab191606
SERCA2a	Abcam	Cat#ab150435
STAT3	Abcam	Cat#ab68153
TNF- α	Abcam	Cat#ab205587
ZO-1	Proteintech	Cat#21773-1-AP
ZO-2	Proteintech	Cat#18900-1-AP
α -SMA	Abcam	Cat#ab124964
β -actin	Affinity Biosciences	Cat#AF7018
812 embedding agent	SPI	Cat#90529-77-4
MiniBEST Kit	Takara	Cat#9767
Osmic acid	Ted Pella Inc	Cat#18,456
PrimeScript Kit	Takara	Cat#RR047 A
TB Green Kit	Takara	Cat#RR820 A
Instruments	Source	Model
Electroconversion and Electrophoresis instrument	Bio Rad	JY300 C
Fluorescence microscope	Mshot	MF43
Centrifuges	Jouan SA	MR1822
Microplate reader	TECAN	Infinite F50
Nucleic acid protein analyzer	BioDrop	BioDrop Duo
Photomicrography system	OLYMPUS	DP73
RT-qPCR instrument	Agilent	Stratagene Mx3000P
Color doppler ultrasound system	Visual Sonics	Vevo 2100
Electrocardiogram	Fukuda	FX7202
Respirator	Chengdu Taimeng Technology	HX-100E
Transmission electron microscope	HITACHI	HT7800/ HT7700
Ultra high performance liquid chromatograph	Agilent	Agilent 1290 Infinity II
Microplate spectrophotometer	Bio TEK	Epoch
UPV INC gel image analysis system	Tanon	ASDF-67PU

Table 4. Materials and equipment utilized in this research.

to 25%B; from 55 to 57 min, 25%B to 28%B; from 57 to 65 min, 28%B; and from 65 to 70 min, 28%B to 100%B. The flow speed was kept at 0.6 ml/min, with the column temperature set to 30°C. The wavelength of the Diode Array Detector (DAD) was set at 280 nm. The injection volume was kept at 2 μ l.

Methodological Evaluation: Precision, Stability, and Repeatability Assessment: A batch of KTBA decoction (S1) was utilized to prepare the test solution following the specified method. The solution was injected six times under the established chromatographic conditions at intervals of 0, 2, 4, 8, 12, and 24 h post-preparation, with the chromatograms duly recorded. The Chinese Medicine Chromatographic Fingerprint Similarity Evaluation Software (version 2004) was employed for common peak matching, facilitating the calculation of retention time, relative standard deviation (RSD) of peak area, and chromatographic similarity for each common peak. The findings indicated that 38 common peaks were identified across the six samples. The RSD of retention time for each common peak was below 0.10%, the RSD of peak area was under 2.0%, and the chromatographic similarity exceeded 0.998. These results demonstrate that the instrument exhibits high precision, the sample maintains stability for up to 24 h, and the method displays excellent repeatability.

Establishment of the Fingerprint Spectrum: Ten batches of KTBA decoction were analyzed. The test solutions were prepared following the previously described method and analyzed under the specified chromatographic conditions, with chromatograms recorded accordingly. The chromatographic data were imported into the Chinese Medicine Chromatographic Fingerprint Similarity Evaluation System (2004 version). Chromatographic peaks occurring before 70 min were excluded. Spectrum S1 was designated as the reference spectrum, and the median method was employed to align common peaks, resulting in the generation of a control spectrum. The chromatograms of the ten sample batches were then matched against the control spectrum to calculate similarity indices. The analysis identified 38 common peaks within KTBA decoction, as illustrated in **Figures S1.A and S1.B**. The similarity indices between the sample batches and the control spectrum ranged from 0.996 to 0.999, as detailed in **Table S2**.

Model preparation

After a week of acclimatization, 91 healthy male Sprague-Dawley (SD) rats were randomly divided into two groups using a random number table: a sham-operation group with 10 rats and an experimental group with 81 rats. To model chronic HF, the left anterior descending (LAD) coronary artery was tied off, followed by exhaustive swimming and starvation. The LAD sham-operation rats were punctured but not tied off, and the post-surgery protocol matched that of the experimental group. The experimental group, on the other hand, underwent LAD ligation. Following a 12-hour fasting period, the rats were anesthetized via an intraperitoneal injection of 3% pentobarbital at a dosage of 50 mg per kilogram of body weight. Afterward, the rats were fastened to a pad, their chests were shaved and cleaned, and they were intubated and connected to a positive pressure ventilator. The ventilator settings included a tidal volume of 6 mL, a respiratory ratio of 2:1, and a rate of 80 breaths per minute. An electrocardiogram (ECG) was taken (Fig. 7B-**Lead I A and Lead II A**). After additional sterilization, a thoracotomy between the left third intercostal and left fourth intercostal spaces exposed the heart's left atrial appendage. A 4–0 suture needle was used to tie off the region 2 mm beneath the LAD. Visually, the blood supply area of the LAD appears pale. Another ECG was performed to confirm heightened ST segment (Fig. 7B-**Lead I B and Lead II B**). After the ligation, we quickly squeeze the chest cavity to expel air and suture it layer by layer with surgical sutures to close the chest cavity. The ventilator was deactivated upon the restoration of spontaneous breath. Post-surgery, the rats were returned to their original cages once their breathing and cardiac rhythms stabilized. Out of 81 rats that underwent coronary ligation, 58 survived, accounting for 71.6% of the total rats. All rats were subjected to an adaptive feeding regimen of a normal diet for one week, during which they were provided unrestricted access to water. Concurrently, they received daily intraperitoneal injections of 8×10^5 U of penicillin to mitigate the risk of infection for a week. Following the adaptive feeding period, the quantity of feed was reduced by half. The rats were then subjected to exhaustive swimming to induce fatigue (a plastic bucket with a diameter of 1 m and a depth of 78 cm was prepared, and warm water at around 35°C was poured in. The exhaustion standard was to submerge the rat's head completely in the water for 5 seconds with no obvious movement of its limbs. If each rat experienced exhaustion three times, it was removed, and the soaked rats were wiped dry with a towel, then dried with a hair dryer, and returned to the cage). This procedure was done daily. After four weeks, an echocardiogram was carried out. The chronic HF model was considered effective if ejection fraction (EF) was 45% or lower¹⁰².

Grouping and dosing

The 51 models left, showing a EF of 45% or lower, were chosen and then randomly split into five separate experimental groups. This study included 10 rats each for the model, tolvaptan, KTBA, and KTBA + S groups, 11 for the KTBA + P group, and 10 for the sham group. Previous studies by our team have shown that the rat equivalent dose of KTBA decoction, when adjusted to the human clinical dose, provides the best therapeutic outcomes^{51–53}. As a result, KTBA decoction was not categorized into low, medium, and high doses^{61,102}. Tolvaptan is frequently used for the clinical management of chronic HF¹. The rat dosage is equivalent to X mg/kg (human dose) multiplied by 70 kg and then by 0.018/0.2 kg. The sham and model groups received normal saline via gavage. The tolvaptan group was given 1.35 mg/kg/day of tolvaptan, while the KTBA group received 15.75 g/kg/day of KTBA decoction, both via gavage. The KTBA + S group received the same KTBA dose plus a 1.5 mg/kg/day intraperitoneal injection of SB203580. The KTBA + P group received the same KTBA dose plus a 120 mg/kg/day intraperitoneal injection of PDTC. Each group received 3 ml per dose, administered twice a day, over a period of four weeks. The observed death counts were: one rat in the model, tolvaptan, and KTBA + S groups, respectively, and two in the KTBA and KTBA + P groups, respectively.

Urinary output

Following the four-week administration period, the rats were removed from their respective cages and subjected to a 12-hour fasting period prior to being placed in their metabolic cages. Each rat was then situated in a metabolic cage, devoid of any food but with ample water supply. Over the course of 24 h, urine was collected using the metabolic cage, and the total 24-hour urinary output (ml) for each rat was recorded.

Histological examination

After four weeks of treatment, Rats were anesthetized by intraperitoneal injection of 3% pentobarbital sodium, and after losing consciousness, aortic blood was collected to induce euthanasia. The abdomen was opened, the diaphragm punctured, and the heart and brain were removed and rinsed with saline. Samples from the heart's border zone and the hippocampus were collected. These tissues were fixed in 4% paraformaldehyde for 48 h, then washed, dehydrated using a series of alcohol concentrations (70%→80%→90%→95%→100% (I)→100% (II)), and cleared with xylene. The tissues were embedded in paraffin, cooled, solidified, sliced into 4 µm sections, mounted on slides, and dried at 50°C.

1) HE staining: The dried slices were treated with xylene I and II for 10 min each, deparaffinized, and gradually dehydrated with alcohol concentrations (100% 30 s→100% 2 min→95% 2 min→85% 2 min→75% 2 min). They were soaked in tap water for 5 min, stained with hematoxylin for 2 min, differentiated with 0.1% hydrochloric acid ethanol for 30 s, and rinsed to return to blue. After drying, they were stained with eosin for 1 min, washed, and dehydrated with alcohol concentrations (95% 1 min→95% 1 min→100% 2 min→100% 2 min). The slices were made transparent with xylene I and II for 10 min each and sealed with neutral resin to observe pathological changes in myocardial and hippocampal tissues.

2) Masson staining: Myocardial slices undergo dewaxing, water treatment, and are stained with Weigert hematoxylin for 5 min. Differentiate with acetic acid for 2 min, wash, and stain with Ponceau S acid fuchsin for 5 min. Soak in weak acid solution for 1 min, wash with phosphomolybdic acid for 1 min, and rinse again with weak acid solution. Immerse in aniline blue for 1 min, clean with weak acid solution, and dehydrate with ethanol of varying concentrations for 5 s each. Clear with xylene three times for 2 min each, then seal with neutral resin to examine myocardial fibrosis.

3) Sirius staining: Myocardial slices were subjected to conventional dewaxing and water treatment. Wash twice with PBS, each time for 5 min. Remove excess water, add Sirius Red staining solution onto sliced tissue, and place in a wet box for 1 h. Wash twice with PBS, each time for 5 min, rinse with running water to remove excess Sirius Red staining solution from the surface. Xylene undergoes conventional dehydration and transparency treatment. After sealing, it is observed under a microscope.

4) Nissl staining: Brain tissue slices were subjected to conventional dewaxing and water treatment. After differentiation with Nissl differentiation medium for 2 min, the slices were washed twice with PBS, dehydrated with a series of graded ethanol solutions, made transparent with xylene, and sealed with neutral gel. The hippocampal CA1 region was then observed under a microscope.

Immunohistochemistry staining

Paraffin-embedded heart tissue sections were analyzed for collagen I, collagen III, α-SMA, SERCA2a, and phospholamban expression using immunohistochemistry.

- a. Dewaxing: Myocardial slices underwent standard dewaxing and water treatment.
- b. Microwave thermal repair: Immerse slices in citrate buffer (pH 6.0), microwave on high for 5–8 min, cool for 20 min, microwave on medium for 2–3 min, cool for 20 min, rinse with ddH₂O for 2 min, then PBS for 2 min.
- c. Endogenous peroxidase block: Incubate slices in 3% hydrogen peroxide at room temperature for 30 min, avoiding light. Wash with PBS three times for 5 min each.
- d. Non-specific staining block: Use 5% BSA for 30 min.
- e. Primary antibody incubation: Store slices overnight at 4°C with 50 µl primary antibodies (collagen I:1/500, collagen III:1/1000, α-SMA:1/1000, SERCA2a:1/100, phospholamban:1/1000) in a wet box.
- f. Secondary antibody incubation: Wash with PBS for 5 min, three times, then cover tissue with enzyme-labeled secondary antibody polymer reagent (1/200) at 37°C for 50 min in a wet box.
- g. Apply DAB stain, observe under a microscope, rinse with ddH₂O, stop staining, and soak in tap water for 5–15 min.
- h. Counterstain with hematoxylin for 2 min and rinse with running water for 10 min.
- i. Dehydrate with gradient alcohol: 70% for 1 min, 80% for 1 min, 90% for 1 min, 95% twice for 5 min each, and 100% twice for 5 min each. Clear with xylene twice for 10 min each and seal with neutral resin.
- j. Randomly select and photograph 3 fields of view per slice under an optical microscope. Calculate the average positive area using Image J software for reflecting the relative protein levels of collagen I, collagen III, α-SMA, SERCA2a, and phospholamban.

Transmission Electron microscope examination

Add electron microscopy solution to the culture dish, take an appropriate amount of hippocampal and heart tissues, and use a surgical knife to cut it into 1 mm³ small pieces. Hippocampal and cardiac tissues were sectioned into ultra-thin slices of 1–2 µm thickness using a microtome. The sections were initially fixed with 2.5% glutaraldehyde, followed by rinsing with PBS containing 0.1% Tween-20. Subsequently, the sections were fixed in 1% osmium tetroxide (pH 7.4) for 2.5 h, protected from light. Dehydration was performed using a graded series of ethanol and acetone, progressing from 30 to 100% ethanol (30%→50%→70%→80%→95%→100%), with each step lasting 20 min, followed by two 15-minute immersions in 100% acetone. The tissues were then embedded in a mixture of acetone and embedding medium, cured overnight, and polymerized for 48 h at 60 °C using

embedding molds. Ultra-thin sections of 50–60 nm were obtained using an ultra-microtome and mounted onto 150 mesh copper grids coated with aromatic film. The sections were stained with uranyl acetate and lead citrate. Specifically, the grids were stained in a 2% uranyl acetate saturated alcohol solution in the dark for 8 min, rinsed three times each with 70% alcohol and ultrapure water, then stained with a 2.6% lead citrate solution in the dark for 8 min, followed by three washes with ultrapure water. The grids were gently dried with filter paper and left to dry overnight at room temperature in a copper grid box. The ultrastructure of the hippocampus and myocardium was observed using a Hitachi transmission electron microscope at 80 kV.

Reverse transcription quantitative real-time polymerase chain reaction

Total RNA Extraction: Use the MiniBEST Universal RNA Extraction Kit. Grind 50–100 mg of hippocampus tissue in a mortar with liquid nitrogen, repeating three times. Add lysis buffer, centrifuge, collect supernatant, wash, and add nuclease-free water to obtain total RNA. Measure RNA concentration with a BioDrop analyzer.

Reverse Transcription: ① Use the PrimeScript[®] RT reagent kit with gDNA Eraser. For DNA removal, mix 0.5 µg RNA with 5×gDNA Eraser Buffer 2 µl, gDNA Eraser 1 µl, add nuclease free water to 10 µl, and incubate at 42 °C for 2 min. ② For reverse transcription, add 5×PrimeScript[®] Buffer 2(for Real Time)4 µl, PrimeScript[®] RT Enzyme Mix I 1 µl, RT Primer Mix 1 µl (specific reverse transcription primers are used for reverse transcription of small RNAs), and RNase-free H₂O 4 µl to 10 µl of the reaction solution from step①. Incubate at 37 °C for 15 min, then 85 °C for 5 s. Store cDNA at 4 °C.

QPCR: For detection, the Stratagene Mx3000p fluorescence quantitative PCR instrument (Agilent Technologies) was utilized. The TB Green[®] Premix Ex Taq[™] II (Tli RNaseH Plus) reagent kit (Takara) was employed for the reactions. The reaction mixture comprised 10 µl of 2×Master Mix, 5.7 µl of RNase-Free H₂O, 0.3 µl of control fluorescent dye, 1 µl each of upstream and downstream primers(primer designed using Primer BLAST, each primer sequence is shown in **Table S3**), and 2 µl of reverse transcription product cDNA. The thermal cycling conditions were as follows: an initial denaturation at 95 °C for 3 min; denaturation at 95 °C for 5 s, followed by annealing at 60 °C for 1 min, with fluorescence signals collected over 40 cycles. Post-cycling, the melting curve was assessed under the following conditions: 95 °C for 15 s, 55 °C for 1 min, and 95 °C for 30 s. During the temperature increase from 55 °C to 95 °C, fluorescence signals were recorded at 0.5 °C increments. Initially, gradient-diluted cDNA templates were used to evaluate the amplification efficiency of each primer. Quantitative PCR detection was conducted on each sample group, and upon completion, the specificity of the PCR reaction was confirmed via the melting curve analysis. Calculate the relative expression levels of p38MAPK, NF-κB, I-κBa, AQP4, ZO-1, and Occludin mRNA in each sample using the following formula, where E_{target} is the amplification efficiency of the target gene, E_{ref} is the amplification efficiency of the reference gene, and Δ Ct is the difference between the Ct values of the control group and the sample.

$$\text{ratio} = \frac{(1 + E_{\text{target}})^{\Delta Ct_{\text{target(control-sample)}}}}{(1 + E_{\text{ref}})^{\Delta Ct_{\text{ref(control-sample)}}}}$$

Western blot

Protein Sample Processing: Extract approximately 30 mg of frozen hippocampal tissue, cut into pieces, and grind in a 5 mL EP tube. Prepare RIPA lysis buffer (RIPA with PMSF at 100:1 ratio, mix 1 ml RIPA with 0.01 ml PMSF shortly before use), adding 10 µL per 1 mg of tissue. Homogenize on ice, then let it stand in a 4 °C fridge until fully lysed. Centrifuge at 4 °C for 15 min at 12000r/min and collect the supernatant as the protein extract. Use BCA to measure concentrations per the reagent kit instructions (from Beyotime Biotechnology Co., Ltd.). Calculate the volume needed to obtain 40 µg of protein based on concentration. For instance, if each sample is 10 µL, 400 µL allows for 40 loads (200/400 at once). For protein denaturation, use the formula x*40 + 80 loading buffer, and prepare 400 µL with dd water, adding 1/5 of the total volume as loading buffer. Mix well and heat in boiling water for 5 min. After sufficient denaturation of the protein, cool to room temperature and centrifuge for a few seconds. Store in a -80 °C freezer for later use.

SDS-PAGE Gel Preparation and Electrophoresis: Prepare the separation gel as per kit instructions, pour it, and level with ethanol. Let it set for 15 min. Remove ethanol, add the stacking gel, insert the comb, and let it set for another 15 min. For electrophoresis, secure the gel on the rack, fill the tank with buffer, ensuring the middle is higher than the sides. Load protein samples and markers, set voltages to 80 V for the stacking gel and 120 V for the separation gel, and run for 1–2 h.

Transmembrane Procedure: Activate a polyvinylidene fluoride (PVDF) membrane with methyl alcohol for 5 min. Prepare an enamel tray with a film transfer clip, two sponge pads, and six layers of filter paper, then soak in film transfer buffer. Equilibrate a rubber strip in the buffer for 15–30 min. Assemble the rotating film clips in this order from bottom to top: black clip, sponge, three-layer filter paper, gel, PVDF membrane, three-layer filter paper, sponge, and white clip. Electrotransfer the protein onto the PVDF membrane.

Sealing PVDF Membrane: Seal the membrane with 5% non-fat milk powder or 5% BSA for 2 h. Rinse the membrane with TBST three times for 10 min each. **Primary Antibody Incubation:** Incubate the PVDF membrane with primary antibodies [AKT (1:1000), p-AKT(1:1000), TNF(1:1000), STAT3(1:1000), p38(1:1000), p-p38(1:1000), I-κBa(1:1000), p-I-κBa(1:1000), p65 (1:1000), p-p65(1:1000), AQP4(1:1000), Occludin(1:1000), ZO-1(1:2000), β-actin(1:1000)] at room temperature for 60 min, overnight at 4 °C, and then at room temperature for 60–120 min the next day. Collect the primary antibody solution and rinse the membrane with TBST three times for 10 min each, shaking in between.

Secondary Antibody Incubation: Dilute the secondary antibody in 5% non-fat milk powder at a 1:10000 ratio. Put secondary antibody in an incubation container. Let it sit at ambient temperature for 60–120 min while shaking the platform. Reuse the solution containing the secondary antibody. Repeat the TBST rinse process thrice. The PVDF membrane was automatically exposed and imaged after dropping ECL chromogenic agent. The proportional amounts of the target proteins were determined by the equation: Relative levels of the target protein are calculated as the ratio of its quantified value to that of β-actin.

In vitro(Fig. 7C and D)

Culture

Remove CCD-841 CoN cells (Guang Zhou Jennio Biotech Co., Ltd.; No. 2021080955301) from the -80 °C freezer and thaw them in a 37 °C water bath. Once fully thawed, visually inspect and retrieve the CCD-841 CoN cells. The experimental procedure is as follows: (1) Transfer the thawed cell suspension into a centrifuge tube containing high-glucose culture medium; (2) Mix thoroughly by pipetting and centrifuge at 1500 rpm for 2 min; (3) Discard the supernatant and add fresh high-glucose culture medium. Inoculate the resuscitated CCD-841 CoN colon epithelial cells into culture dishes and flasks at a specified concentration, and incubate them in an incubator using Dulbecco's Modified Eagle Medium (DMEM) (Gibco, Thermo Fisher Scientific, NYC, USA) supplemented with 10% fetal bovine serum (FBS) (Gibco, Thermo Fisher Scientific, NYC, USA), maintained at 37 °C in a 5% CO₂ atmosphere. Cells were subcultured into new culture dishes every 2–3 days and discarded post-experimentation. The Cell Counting Kit-8 (CCK-8) assay from APExBIO was employed to construct the cell growth curve.

Model preparation

Create a model of ischemia and hypoxia by employing physical techniques and using DMEM without FBS and glucose to formulate an ischemic solution. In a 37 °C incubator with hypoxic conditions (94% N₂, 5% CO₂, and 1% O₂), substitute the CCD-841 CoN cell culture medium with this mixture. Cultivate for 6, 12, 24, and 36 h respectively, and select the optimal time point for establishing an ischemia hypoxia model. By using western blot for HIF-1α detection (Note: HIF-1α is a hypoxia sensitive molecule.) and CCK-8 assays for cell viability, the model can be validated.

Drug preparation

1) Furosemide (20 mg) was bought from Shanghai Zhaohui Pharmaceutical (Lot No. 2303007) and dissolved in double distilled water to create a 0.72 mg/ml solution.

2) Tanshinone IIA (Tan IIA), derived from the Chinese herb *Salvia miltiorrhiza* Bunge, was sourced from Shanghai Yuanye Bio-Technology (Lot No. S31459). The identification of the plant was verified through the global checklist (<http://mpns.kew.org>). Previous studies have shown that Tan IIA, in different doses (0, 2.5, 5, 10, and 20 μmol/L), inhibits the growth of synovial fibroblast cells¹⁰³. Additionally, Tan IIA has been found to suppress the growth of NSCLC cells in a concentration-dependent way at levels of 1.25, 2.5, 5, 10, 20, and 40 μmol/L¹⁰⁴. Furthermore, Tan IIA at doses of 0, 1, 5, 10, and 20 μmol/L has been demonstrated to suppress apoptosis in SW480 colorectal cancer cells in a dose-dependent fashion¹⁰⁵. As a result, different concentrations of Tan IIA, specifically 1.25 μmol/L, 2.5 μmol/L, 5 μmol/L, 10 μmol/L, and 20 μmol/L, were prepared using DMSO. The viability of the cells was subsequently assessed through the CCK-8 assay. All pharmaceutical substances were preserved at a temperature of 4 °C.

Grouping and dosing

Choose logarithmic phase cells and divide into nine groups:

- 1) Control group: DMEM culture medium plus control small interfering ribonucleic acid (siRNA);
- 2) Model group: DMEM culture medium plus control siRNA;
- 3) Furosemide group: 0.72 mg/ml furosemide solution plus control siRNA;
- 4) Tan IIA-low-dose (Tan IIA-L) group: 2.5 μmol/L Tan IIA;
- 5) Tan IIA-medium-dose (Tan IIA-M) group: 5 μmol/L Tan IIA plus control siRNA;
- 6) Tan IIA-high-dose (Tan IIA-H) group: 10 μmol/L Tan IIA;
- 7) Tan IIA-M + p38 si group: 5 μmol/L Tan IIA plus p38MAPK siRNA;
- 8) Tan IIA-M + p65 si group: 5 μmol/L Tan IIA plus p65 NF-κB siRNA;
- 9) Tan IIA-M + AQP4 si group: 5 μmol/L Tan IIA plus AQP4 siRNA.

Transfection

Inoculate an appropriate proportion of cells into a cell culture plate one day prior to transfection, as specified in **Table S4**. It is recommended to achieve a cell density of 70–90% confluence by the second day of transfection.

- a. Dilute 60 pmol, 80 pmol, and 100 pmol of SiRNA in 25 μl of serum-free medium and mix thoroughly.
- b. Dilute 1 μl, 1.2 μl, and 1.5 μl of HG TransGene™ transfection reagent in 25 μl of serum-free medium and mix thoroughly.

c. Prepare various proportions of the SiRNA-transfection reagent mixture by combining the SiRNA Dilution from step **a** with the HG TransGene™ transfection reagent Dilution from step **b**, and allow the mixture to stand at room temperature for 15–20 min.

d. Introduce the prepared siRNA-transfection reagent complex into the culture well containing the cells and complete culture medium. Gently agitate the culture plate horizontally in all directions to ensure even mixing.

e. Incubate the cells at 37 °C, replace the medium after 4–6 h, and continue cultivation for an additional 24 h prior to assessing transfection efficiency using a Nikon fluorescence microscope.

f. Choose the transfection concentration with high efficiency and cell survival from the optimized results. Prepare the siRNA-transfection reagent mixture as each experimental group. Replace the serum-containing medium with PBS, then add 0.5 ml of serum-free DMEM. Mix in the siRNA transfection reagent and incubate under 5% CO₂ at 37 °C.

Western blot

Dissolve the RIPA protein hydrolysate at ambient temperature and incorporate a mixture of protease and phosphatase inhibitors. Ensure thorough mixing, then promptly place the solution on ice. Wash the cells 2–3

times with PBS that has been pre-cooled to 4 °C. Treat the cells with trypsin to prevent adherence to the container walls, and use a pipette to detach and remove the cells. Collect the cells by centrifugation, carefully aspirate the supernatant, and retain the cell pellet for subsequent use. Add 100 µL of lysis buffer to a concentration of 1×10^6 cells, incubate on ice for 5 min, and sonicate in an ice bath for 20 s using an ultrasonic device. For extraction, centrifuge at 12,000 rpm and 4 °C for 10 min. Immediately transfer the supernatant to a pre-cooled 1.5 mL EP tube to isolate the extracted cellular protein. The subsequent procedures were consistent with those employed in *in vivo* experiments.

Immunofluorescence staining

An immunofluorescence assay was conducted to examine p38MAPK, p65 NF-κB, and AQP4 expression and localization in CCD-841 CoN cells. Cells were placed in a 24-well plate on a glass slide, grouped, and allowed to adhere. A physical ischemia and hypoxia model was created, and cells were treated with Tan IIA-M, Furosemide, Tan IIA-M + p38 siRNA, Tan IIA-M + p65 siRNA, or Tan IIA-M + AQP4 siRNA for 48 h. After removing the slide, cells were fixed with 4% paraformaldehyde, incubated with primary antibodies at 4 °C for 12 h, and with secondary antibodies at room temperature for 1 h. DAPI was used to stain nuclei, and the slide was sealed and observed under a Nikon fluorescence microscope.

- a. Soak the clean cover glass in 70% ethanol, then place it in a culture dish using sterile tweezers, and rinse with sterile PBS. Seed CCD-841 CoN cells in a 24-well plate at 5000–7000/cm² and incubate at 37 °C with 5% CO₂ until 80% confluence.
- b. Remove the cover glass and fix with 4% paraformaldehyde for 15 min. Wash three times with PBS for 3 min each.
- c. Incubate cells in 0.3% Triton X-100 in PBS at room temperature on a shaker for 10 min.
- d. Wash the slide three times with PBS for 3 min each, dry with absorbent paper, and apply blocking buffer (10% goat serum with 0.1% Tween-20 in PBS). Block for 60 min at room temperature.
- e. Use absorbent paper to remove the blocking solution, apply primary antibodies [p38MAPK (1/500), p65 NF-κB (1/400), AQP4 (1/200)] to each slide, and incubate in a wet box overnight at 4 °C. Wash off the primary antibodies with PBST (0.1% Tween-20 in PBS) on a shaker for 5 min, repeating three times.
- f. After removing the wash solution with absorbent paper, add fluorescent secondary antibody (1:1000), incubate in a wet box for 1 h, then wash three times with PBST for 5 min each, avoiding light exposure.
- g. Apply DAPI to stain the nucleus for 5 min in the dark, then wash three times with PBST for 5 min each to remove excess DAPI.
- h. Dry the slide with absorbent paper, seal with an anti-fluorescence quencher solution, and observe under a fluorescence microscope.

Reverse transcription quantitative Real-Time polymerase chain reaction

The CCD-841 CoN cells were gathered via a process involving digestion and centrifugation, which was followed by a procedure identical to that employed in *in vivo* experiments. The PCR primer sequence is listed in **Table S3**.

Statistical analysis

SPSS 22.0 or GraphPad Prism 9.3.0 were used for statistical evaluations. Normally distributed data are shown as mean ± standard deviation and compared using one-way ANOVA. The LSD method was used for homogeneous variance pairwise comparisons, while the Dunnett T3 method was used for non-homogeneous ones. Non-parametric tests were used for non-normally distributed data comparisons. A $p < 0.05$ and $p < 0.01$ indicated that the difference was statistically significant.

Data availability

The data that support the findings of this study are available from the corresponding author upon reasonable request.

Received: 30 September 2024; Accepted: 5 May 2025

Published online: 29 May 2025

References

1. McDonagh, T. A. et al. ESC scientific document group.2021 ESC guidelines for the diagnosis and treatment of acute and chronic heart failure. *Eur. Heart J.* **42** (36), 3599–3726. <https://doi.org/10.1093/euhr/eabt368>(2021). ,Mebazaa,A.,Mindham,R.,Muneretto,C.,Francesco Piepoli,M.,Price,S.,
2. Bolognese, L. et al. D.Left ventricular remodeling after primary coronary angioplasty:patterns of left ventricular dilation and long-term prognostic implications.*Circulation.*106,2351–2357.<https://doi.org/10.1161/01.CIR.0000036014.90197.FA>. (2002).
3. Frantz, S., Hundertmark, M. J., Schulz-Menger, J., Bengel, F. M. & Bauersachs J.Left ventricular remod- Elling post-myocardial infarction:pathophysiology,imaging, and novel therapies. *Eur. Heart J.* **43** (27), 2549–2561. <https://doi.org/10.1093/eurheartj/eha c223>(2022).
4. Tsao, C. W. et al. Heart Disease and Stroke Statistics-2023 Update: A Report From the American Heart Association. *Circulation* **147** (8). <https://doi.org/10.1161/CIR.0000000000001123>(2023). & American Heart Association Council on Epidemiology and Prevention Statistics Committee and Stroke Statistics Subcommittee
5. Conrad, N. et al. K.Temporal trends and patterns in heart failure incidence:a population-based study of 4 million individuals.*Lancet.*391(10120)572–580 (2018). [https://doi.org/10.1016/S0140-6736\(17\)32520-5](https://doi.org/10.1016/S0140-6736(17)32520-5)
6. Priyadarshi, R., Ranjan, R., Kumar Vishwakarma, A., Yang, T. & Rathore, R. S. Exploring the frontiers of unsupervised learning techniques for diagnosis of cardiovascular disorder: A systematic review. *IEEE Access.* **12**, 139253–139272. <https://doi.org/10.1109/ACCESS.2024.3468163> (2024).
7. Williams, L. R. & Leggett R.W.Reference values for resting blood flow to organs of man. *Clin. Phys. Physiol. Meas.* **10**(3),187–217 <https://doi.org/10.1088/0143-0815/10/3/001>(1989).

8. Ackerman, R. H. Cerebral blood flow and neurological change in chronic heart failure. *Stroke*. **32** (11), 2462–2464 (2001).
9. Sandek, A. et al. vonHaehling,S.D. J.Intestinal blood flow in patients with chronic heart failure: a link with bacterial growth, Gastrointestinal symptoms, and cachexia. *J. Am. Coll. Cardiol.* **64**(11)1092–1102 <https://doi.org/10.1016/j.jacc.2014.06.1179> (2014).
10. Boccella, N. et al. C. Transverse aortic constriction induces gut barrier alterations, microbiota remodeling and systemic inflammation. *Sci. Rep.* **11** (1). <https://doi.org/10.1038/s41598-021-86651-y> (2021).
11. Fulop, G. A. et al. & Ungvari,Z.Cerebral venous congestion promotes blood-brain barrier disruption and neuroinflammation, impairing cognitive function in mice. *Geroscience* **41**(5)575–589 <https://doi.org/10.1007/s11357-019-00110-1> (2019).
12. Shayez Karim, S. M., Md Shah, F. & Rathore R.S.Identifying discriminative features of brain network for prediction of Alzheimer's disease using graph theory and machine learning. *Front Neuroinform.* (2024). <https://doi.org/10.3389/fninf.2024.1384720>
13. Zhu, Y. et al. W.Gut microbiota meta- bolites as integral mediators in cardiovascular diseases(Review). *Int. J. Mol. Med.* **46** (3), 936–948. <https://doi.org/10.3892/ijmm.2020.4674> (2020).
14. Doehner, W., Čelutkienė,J.,Yilmaz, M. B. & Coats, A. J. S. Heart failure and the heart-brain axis. *QJM* **116** (11), 897–902. <https://doi.org/10.1093/qjmed/hcad179> (2023).
15. Raman, M., Chen, W. & Cobb, M. H. Differential regulation and properties of MAPKs. *Oncogene* **26** (22), 3100–3112. <https://doi.org/10.1038/sj.onc.1210392> (2007).
16. Liu, P. Q. et al. Role and mechanisms of the NF-κB signaling pathway in various developmental processes. *Biomed. Pharmacother.* **153**, 113513. <https://doi.org/10.1016/j.bioph.2022.113513> (2022).
17. Abdullah, M., Berthiaume, J. M. & Willis M.S.Tumor necrosis factor receptor-associated factor 6 as a nuclear factor kappa B-modulating therapeutic target in cardiovascular diseases:at the heart of it all. *Transl Res.* **195**,48–61 <https://doi.org/10.1016/j.trsl.2017.10.012> (2018).
18. Oeckinghaus, A. & Ghosh S.The NF-κappaB family of transcription factors and its regulation. *Cold Spring Harb Perspect. Biol.* <https://doi.org/10.1101/cshperspect.a000034> (2009).
19. Zhang, M. et al. X.Uncovering the molecu- Lar mechanisms of curcumae rhizoma against myocardial fibrosis using network Pharmacology and experimental validation. *J. Ethnopharmacol.* **115751** <https://doi.org/10.1016/j.jep.2022> (2023).
20. See, F. et al. H.p38mitogen- activated protein kinase Inhibition improves cardiac function and attenuates left ventricular remodeling following myocardial infarction in the rat. *J. Am. Coll. Cardiol.* **44**(8)1679–1689 <https://doi.org/10.1016/j.jacc.2004.07.038>(2004).
21. Zhang, Y. et al. S.Z.The protective role of liquiritin in high fructose-induced myocardial fibrosis via inhibiting NF-κB and MAPK signaling pathway.*Biomed Pharmacother.***84**,1337–1349 <https://doi.org/10.1016/j.bioph.2016.10.036>(2016).
22. Frigeri, A., Gropper, M., Turck, C. W. & Verkman, A. S. Immunolocalization of the mercurial-insensitive water channel and glycerol intrinsic protein in epithelial cell plasma membranes. *Proc. Natl. Acad. Sci. Sci. USA.* **92**, 4328–4331. <https://doi.org/10.1073/pnas.92.10.4328> (1995).
23. Kitchen, P. et al. Aquaporin-4 Subcellular Localization to Treat Central Nervous System Edema. *Cell.* **181**(4),784–799. (2020). <https://doi.org/10.1016/j.cell.2020.03.037>.
24. Tan, C. J. et al. X.S.Xinshuitong Capsule attenuates doxorubicin-induced myocardial edema via regulation of cardiac aquaporins in the chronic heart failure rats.*Biomed Pharmacother.* (2021). <https://doi.org/10.1016/j.bioph.2021.112261>.
25. Li, C., Pan, J. S. P. W. S., Wang, S., Feng, W. & Chen, S. Chai,X.,Zhao,S.&Zhu,X.Ketogenic Diet Alleviates Hypoglycemia- Induced Neuroinflammation via modulation the gut microbiota in mice. *Mol. Nutr. Food Res.* **67** (11), e2200711. <https://doi.org/10.1002/mnfr.202200711> (2023).
26. Bradbury, M. W. & Lightman, S. L. The blood-brain interface. *Eye (Lond.)* **4** (Pt 2),249–254 (1990). <https://doi.org/10.1038/eye.1990.36>
27. Berkes, J., Viswanathan, V. K., Savkovic, S. D. & Hecht, G. Intestinal epithelial responses to enteric pathogens:effects on the tight junction barrier, ion transport, and inflammation. *Gut* **52** (3), 439–451. <https://doi.org/10.1136/gut.52.3.439> (2003).
28. Su, Y. et al. & Yan,T.Activation of Cholinergic Anti-Inflammatory Pathway Ameliorates Cerebral and Cardiac Dysfunction After Intracerebral Hemorrhage Through Autophagy. *Front Immunol.* (2022). <https://doi.org/10.3389/fimmu.2022.870174>.
29. Zhu, H., Dai, R., Zhou, Y., Fu, H. & Meng Q.TLR2 ligand Pam3CSK4 regulates MMP-2/9 expression by MAPK/NF-κB signaling pathways in primary brain microvascular endothelial cells. *Neurochem Res.* **43**(10)1897–1904 <https://doi.org/10.1007/s11064-018-2607-7> (2018).
30. Chen, J., Wei, X. Z. Q., Wu, Y., Xia, G. & Xia, H. Wang,L.,Shang,H.&Lin,S.The traditional Chinesemedicines treat chronic heart failure and their main bioactive constituents and mechanisms. *Acta Pharm. Sin B* **13**(5)1919–1955 <https://doi.org/10.1016/j.apsb.2023.02.005>(2023).
31. Wu, N. X. et al. L.Traditional Chinese medication Qili Qiangxin capsule protects against myocardial ischemia- reperfusion injury through suppressing autophagy via the phosphoinositide 3-kinase/protein kinase B/forkhead box O3 axis traditional Chinese medication Qili Qiangxin capsule protects against myocardial ischemia-reperfusion injury through suppressing autophagy via the phosphoinositide 3-kinase/protein kinase B/forkhead box O3 axis. *J. Ethnopharmacol.* **337**(Pt 1),<https://doi.org/10.1016/j.jep.2024.118821>(2025).
32. Chen, X. F. et al. The mechanism of Renshen-Fuzi herb pair for treating heart failure-Integrating a cardiovascular Pharmacological assessment with serum metabolomics. *Front. Pharmacol.* **13**, 995796. <https://doi.org/10.3389/fphar.2022.995796> (2022).
33. Zhang, Y., He, J., Zhang, W. & Song, T. T. B. Huoxue formula combined with conventional Western medicine for 129 patients of heart failure with Mid-range ejection fraction with syndrome of Qi deficiency and blood stasis:a randomized controlled trial. *J. Tradit. Chin. Med.* **65** (4), 376–381. <https://doi.org/10.13288/j.11-2166/r.2024.04.008> (2024).
34. Liu, S. Y.Exploring the Clinical Efficacy of Kidney-Tonifying and Blood-Activating Traditional Chinese Medicine in the Treatment of Chronic Heart Failure Based on the Heart and Kidney Theory.*Liaoning University of Traditional Chinese Medicine*,Shenyang. (2021). <https://doi.org/10.27213/d.cnki.glnzc.2021.0000216>. Liaoning, n.d.
35. Liu, S. Y., Zhang, Y. & Kong, F. D. E. Exploration of Bushen Huoxue Decoction on energy metabolism of myocardial mitochondria and expression of PGC-1α,NRF-1,mtTFA mRNA in rats with chronic heart failure based on the theory of heart brain kidney Axis.*JOURNAL OF LIAONING UNIVERSITY OF TCM.* **23**(5),22–26 <https://doi.org/10.13194/j.issn.1673-842x.2021.05.007>(2021).
36. Liu, X. & X.Study on the effect of Bushen Huoxue Compound on IL-6. and STAT3 proteins in rats with chronic heart failure.*Liaoning University of Traditional Chinese Medicine*, Shenyang. (2022). [https://doi.org/10.1016/j.jep.2021.114164](https://doi.org/10.27213/d.cnki.glnzc.2022.0000570Liaoning, n.d.
37. Shen, F., Song, Z. X. P. L. L., Wang, B., Peng, D. & Zhu G.Polygonatum sibiricum polysaccharide prevents depression-like behaviors by reducing oxidative stress, inflammation, and cellular and synaptic damage. <i>J. Ethnopharmacol.</i> <a href=) (2021).
38. Yin, X., Wang, B., Li, X., Zhu, C. & Chen P.Effects of Polygonatum sibiricum polysaccharide on JAK/ STAT pathway and myocardial fibrosis in rats with autoimmune myocarditis. *Int. J. Clin. Exp. Pathol.* **37** (1), 26–32 (2021).
39. Dawuti, A. et al. & Fang,L.H.Salvinolic acid A alleviates heart failure with preserved ejection fraction via regulating TLR/Myd88/ TRAF/NF-κB and p38MAPK/CREB signaling pathways. *Biomed. Pharmacother* <https://doi.org/10.1016/j.bioph.2023.115837>(2023).
40. Kim, J. S. et al. M.D.Anti-fibrotic effects of Cuscuta chinensis with in vitro hepatic stellate cells and a thioacetamide-induced experimental rat model. *Pharm. Biol.* **55** (1), 1909–1919. <https://doi.org/10.1080/13880209.2017> (2017).

41. Wang, X. P. et al. Y.Calycosin as a novel PI3K activator reduces inflammation and fibrosis in heart failure through AKT-IKK/STAT3 Axis. *Front. Pharmacol.* <https://doi.org/10.3389/fphar.2022.828061> (2022).
42. Zhang, Y., Du, M., Wang, J. & Liu, P. A. I. V. Relieves Atherosclerosis and Hepatic Steatosis via MAPK/NF-kappaB Signaling Pathway in LDLR(-/-) Mice. *Front Pharmacol.* 13, (2022). <https://doi.org/10.3389/fphar.2022.828161>
43. Liu, L., Ning, B. B., Cui, J. G., Zhang, T. & Chen Y.miR-29c is implicated in the cardioprotective activity of Panax Notoginseng saponins against isoproterenol-induced myocardial fibrogenesis. *J. Ethnopharmacol.* **198**, 1–4 <https://doi.org/10.1016/j.jep.2016.1.2036>(2017).
44. Luo, H. et al. Y.T.Panax Notoginseng saponins modulate the inflammatory response and improve IBD-Like symptoms via TLR/NF-kB and MAPK signaling pathways. *Am. J. Chin. Med.* **49** (4), 925–939. <https://doi.org/10.1142/S0192415X21500440> (2021).
45. Wang, L., Shao,L.Chen, M. Y., Wang, L., Yang, P. & Tan, F. B., ,W.&Huang,W.H.Panax notoginseng Alleviates colitis via the regulation of gut microbiota. *Am. J. Chin. Med.* **51** (1), 107–127. <https://doi.org/10.1142/S0192415X23500076> (2023).
46. Ning, N., Dang, X. Q., Bai, C. Y., Zhang, C. & Wang K.Z.Panax notoginsenoside produces neuroprotection- Tive effects in rat model of acute spinal cord ischemia-reperfusion injury. *J. Ethnopharmacol.* **139**(2)504–512 <https://doi.org/10.1016/j.jep.2011.11.040>(2012).
47. Ren, B. et al. Q.Ginsenoside Rg3 attenuates angiotensin II-induced myocardial hypertrophy through repressing NLRP3 inflammasome and oxidative stress via modulating SIRT1/NF-kB pathway. *Int. Immunopharmacol.* <https://doi.org/10.1016/j.intimp.2021.107841> (2021).
48. Jin, M., Wu, Y., Wang, L., Zang, B. X. & Tan, L. H. Yellow A attenuates Bleomycin-induced pulmonary fibrosis in mice. *Phytother Res.* **30** (4), 577–587. <https://doi.org/10.1002/ptr> (2016).
49. Pan, R. et al. MRC-5 cell activation induced by TGF-β1 by blocking TGF-β1 binding to TβRII. *Front. Pharmacol.* **8**, 264. <https://doi.org/10.3389/fphar.2017.00264> (2017).
50. Shen, S. Y. et al. G.Leonurine attenuates angiotensin II-induced cardiac injury and dysfunction via inhibiting MAPK and NF-κB pathway. *Phytomedicine* <https://doi.org/10.1016/j.phymed.2022.154519>(2023).
51. Xu, R. et al. Effects of Bushen Huoxue compound on ventricular remodeling and expression of AQP4 in myocardium and Colon in rats with heart failure after myocardial infarction. *Chin. J. Inform. TCM* **30**(07)81–87 <https://doi.org/10.19879/j.cnki.1005-5304.202209191>(2023).
52. Xu, R. et al. Effect of Bushen Huoxue Decoction on correlation between intestinal fluid metabolism and colonic NF-κB,Tight junction protein occludin in rats with chronic heart Failure.*LISHIZHEN MEDICINE AND MATERIA MEDICA RESEARCH* **34**(02),265–269 (2023). <https://doi.org/10.3969/j.issn.1008-0805.2023.02.03>
53. He, X. T., Xu, R. & Zhang Y.Effect of Bushen Huoxue recipe on ventricular remodeling and AVP, AQP's expression in heart and brain tissues of rats with heart failure after myocardial infarction. *Chin. J. Experimental Traditional Med. Formulae.* <https://doi.org/10.13422/j.cnki.syfxj.20241424> (2024).
54. Mo, F. Z. & Deng, T. T. Formation of the System of the Properties of the Five Organs.*Modernization of Traditional Chinese Medicine and Materia Medica-World Science and Technology*.12(4), 545–549.<https://doi.org/10.3969/j.issn.1674-3849.2010.04.011>(2010).
55. Cao, H. X. Basic theory of traditional Chinese medicine. Beijing:*China Press of Chinese Medicine* .:77. (2004).
56. Tan, Q., Du, Y. J. & You M.Based on the Kidney-Du Meridian-Brain axis: exploring the research progress of acupuncture and moxibustion in the prevention and treatment of Alzheimer's disease. *Chin. Acupunct. Moxibustion.* **45**, 0004. <https://doi.org/10.13703/j.0255-2930.20240822> (2025).
57. Chi N.Observation of the clinical efficacy of tonifying-kidney and activating-blood compound based on the theory of heart-brain-kidney axis to treat chronic heart failure.*Liaoning University of Traditional Chinese Medicine*, (2020). <https://doi.org/10.27213/d.cnki.glnzc.2020.000158> Liaoning, n.d.
58. Liu, B. H. et al. *J. Integr. Med.* **27**(4)291–299 <https://doi.org/10.1007/s11655-021-3326-5>(2021).
59. Cai, M. et al. D.F.Tongxinluo reduces brain edema and inhibits post-ischemic inflammation after middle cerebral artery occlusion in rats.*J Ethnopharmacol.* **181**,136–145. (2016). <https://doi.org/10.1016/j.jep.01.026>(2016).
60. Sun, Y. C. et al. Y.L.Observation on the therapeutic effect of Bushen Huoxue formula on diuretic resistance in chronic heart failure. *Chin. J. Experimental Traditional Med. Formulae.* <https://doi.org/10.13422/j.cnki.syfxj.20241124> (2024).
61. Zhang & W.Study on the mechanism of the intervention of Kidney-Tonifying. Blood-Activating compound on myocardial fibrosis in chronic heart failure after myocardial infarction based on the Wnt/β-catenin pathway. *Liaoning Univ. Traditional Chin. Med. Shenyang.* <https://doi.org/10.27213/d.cnki.glnzc.2021.000044> (2021). Liaoning, n.d.
62. Zou, W. C. et al. Bushen Huoxue compound mediates SERCA2a and PLB proteins to regulate Endoplasmic reticulum stress and alleviate myocardial injury in rats with chronic heart failure. *Global Traditional Chin. Med.* **16**(5),817–823. <https://doi.org/10.3969/j.issn.1674-1749.2023.05.001>(2023).
63. Jha, S. K. et al. Quality-of-Service- Centric Design and Analysis of Unmanned Aerial Vehicles. *Sensors*.**22**(15), 5477. (2022). <https://doi.org/10.3390/s22155477>
64. Rathore, R. S. et al. whale grey wolf optimization-based novel energy-efficient clustering for EH-WSNs. *J Wireless Com Network.* **101**. (2020). <https://doi.org/10.1186/s13638-020-01721-5> (2020).
65. Ma, X. K., Zhang, L., Gao, F. J., Jia, W. H. & Li C.*Salvia miltiorrhiza* and *Tanshinone IIA* reduce endothelial inflammation and atherosclerotic plaque formation through inhibiting COX-2.*Biomed Pharmacother.* (2023). <https://doi.org/10.1016/j.bioph.2023.115501>
66. Prabhu, S. D. & Frangogiannis, N. G. The biological basis for cardiac repair after myocardial infarction:from inflammation to fibrosis. *Circ. Res.* **119** (1), 91–112. <https://doi.org/10.1161/CIRCR.ESAHA.116.303577> (2016).
67. van den Borne, S. W. et al. ,Narula,N.,Pitt,B.,Hofstra,L.&Narula,J.Molecular imaging of interstitial alterations in remodeling myocardium after myocardial infarction. *J. Am. Coll. Cardiol.* **52**(24)2017–2028 <https://doi.org/10.1016/j.jacc.2008.07.067>(2008).
68. Pan, J. et al. D.Huangqi Shengmai Yin Ameliorates Myocardial Fibrosis By Activating Sirtuin3 and Inhibiting TGF-beta/Smad Pathway.*Front Pharmacol.* (2021). <https://doi.org/10.3389/fphar.2021.722530>
69. MacLennan, D. & Kranias E.Phospholamban: a crucial regulator of cardiac contractility. *Nat. Rev. Mol. Cell. Biol.* **4**, 566–577. <https://doi.org/10.1038/nrm1151> (2003).
70. Gottlieb, S. S. et al. & Hernandez,A.F.Effects of nesiritide and predictors of urine output in acute decompensated heart failure: results from ASCEND-HF(acute study of clinical effectiveness of nesiritide and decompensated heart failure). *J. Am. Coll. Cardiol.* **62**(13)1177–1183 <https://doi.org/10.1016/j.jacc.2013.04.073>(2013).
71. Yadav, S. K. et al. Comparative analysis of signal processing techniques for mental state recognition in Brain-Computer Interfaces(BCI). *Wirel. Pers. Commun.* **131**,1569–1592. <https://doi.org/10.1007/s11277-023-10514-0>(2023).
72. Mao, M. et al. Y.Neuroprotection of rhubarb extract against cerebral ischaemia-reperfusion injury via the gut-brain axis pathway. *Phytomedicine.* (2024). <https://doi.org/10.1016/j.phymed.2023.155254>
73. Wang, Y. et al. & Zhu,Y.Protection against acute cerebral ischemia/reperfusion injury by QiShenYiQi via neuroinflammatory network mobilization.*Biomed Pharmacother.* (2020). <https://doi.org/10.1016/j.bioph.2020.109945>
74. Wang, Y. et al. Y.Synergy of Yiqi and Huoxue components of QishenYiqi formula in ischemic stroke protection via lysosomal/inflammatory mechanisms. *J. Ethnopharmacol.* <https://doi.org/10.1016/j.jep.2022.115301> (2022).
75. Imamura, T. et al. K.Long-Term Tolvaptan Treatment in Refractory Heart Failure.*Circ Rep.*1(10), 431–437. (2019). <https://doi.org/10.1253/circrep.CR-19-0064>
76. Tan, Q. et al. H.Tolvaptan attenuated brain edema in experimental intracerebral hemorrhage. *Brain Res.* **1715**,41–46 <https://doi.org/10.1016/j.brainres.2019.01.033>(2019).

77. Gordon, J. W., Shaw, J. A. & Kirshenbaum L.A.Multiple facets of NF- κ B in the heart: to be or not to NF- κ B. *Circ. Res.* **108** (9), 1122–1132. <https://doi.org/10.1161/CIRCRESAHA.110.226928> (2011).
78. Romero-Becerra, R., Santamans, A. M., Folgueira, C. & Sabio G.p38 MAPK pathway in the heart: new insights in health and disease. *Int. J. Mol. Sci.* **21** (19). <https://doi.org/10.3390/ijms21197412> (2020).
79. Kang, Y. M., Ma, Y., Elks, C., Zheng, J. P. & Francis J.Cross-talk between cytokines and renin-angiotensin in hypothalamic paraventricular nucleus in heart failure: role of nuclear factor-kappaB. *Cardiovasc. Res.* **79** (4), 671–678. <https://doi.org/10.1093/cvr/cvn119> (2008).
80. Wei, S. G., Yu, Y., Weiss, R. M. & Felder, R. B. I. of Brain Mitogen-Activated Protein Kinase Signaling Reduces Central Endoplasmic Reticulum Stress and Inflammation and Sympathetic Nerve Activity in Heart Failure Rats.*Hypertension*.**67**(1),229–236. <https://doi.org/10.1161/HYPERTENSIONAHA.115.06329>(2016).
81. Yadav, S. K., Jha, S. K., Singh, S., Dixit, P. & Prakash, S. E. Bio-molecules sequencing using Multi-Objective optimization and High-Performance computing. *Wirel. Pers. Commun.* **134**, 1783–1800. <https://doi.org/10.1007/s11277-024-10957-z>(2024).
82. Ishikawa, M., Kobayashi, N., Sugiyama, F., Onoda, S. & Ishimitsu T.Renoprotective effect of vasopressin V2 receptor antagonist Tolvaptan in Dahl rats with end-stage heart failure. *Int. Heart J.* **54** (2), 98–106. <https://doi.org/10.1536/ihj.54.98> (2013).
83. Liu, L. J. et al. Z.Y.Tanshinone IIA attenuates AOM/DSS- induced colorectal tumorigenesis in mice via inhibition of intestinal inflammation.*Pharm Biol.***59**(1),89–96.<https://doi.org/10.1080/13880209.2020.1865412>. (2021).
84. Zhang, Y. G., Ge, T. R., Xiang, P., Zhou, J. Y. & Tang, S. M. Tang.Q.Tanshinone IIA reverses oxaliplatin resistance in human colorectal Cancer via inhibition of ERK/Akt signaling pathway. *Oncotargets Ther.* **12**, 9725–9734. <https://doi.org/10.2147/OTT.S217914> (2019).
85. Zheng, Y. F. et al. M.Q.Effect of Tanshinone IIA on gut Microbiome in Diabetes-Induced cognitive impairment. *Front. Pharmacol.* <https://doi.org/10.3389/fphar.2022.890444>(2022).
86. Wang, K. et al. J.A.Involvement of aquaporin-4 in colonic water absorption and fecal dehydration.*Gastroenterology*.in the Press(1999).
87. Takagi, H. et al. Oiso,Y.Minocycline prevents osmotic demyelination associated with Aquaresis. *Kidney Int.* **86** (5), 954–964. <https://doi.org/10.1038/ki.2014.119> (2014).
88. Wang, C. X. et al. Zhang,P&Cui,X.B.Anti-ascites effect of total saponins of phytolaccae Radix on mice with Ascites and mechanism. *Zhongguo Zhong Yao Za Zhi.* **47** (16), 4411–4417. [\(2022\).](https://doi.org/10.19540/j.cnki.cjcm)
89. Wang, C. et al. C.Mechanism of Aquaporin 4 (AQP4) up-regulation in rat cerebral edema under hypobaric hypoxia and the preventative effect of puerarin.*Life Sci.* **193**,270–281 <https://doi.org/10.1016/j.lfs.2017.10.021>(2018).
90. Jin, X. et al. Y.Involvement of the p38 MAPK signaling pathway in overexpression of matrix metalloproteinase-9 during the course of brain edema in 1,2-dichloroethane-intoxicated mice.*Neurotoxicology*.**69**,296–306.<https://doi.org/10.1016/j.neuro.2018.07.022>. (2018).
91. Yi, X. et al. Zeng,T.,Lu,J.&Han,Z.1-Trifluoromethoxyphenyl-3-(1-Propionylpiperidin-4-yl) Urea Protects the Blood-Brain Barrier Against Ischemic Injury by Upregulating Tight Junction Protein Expression, Mitigating Apoptosis and Inflammation In Vivo and In Vitro Model.*Front Pharmacol.* (2020). <https://doi.org/10.3389/fphar.2020.01197>
92. Zhao, Y. et al. & Fan,H.G.Chlorogenic acid alleviates chronic Stress-Induced intestinal damage by inhibiting the P38MAPK/NF- κ B pathway. *J. Agric. Food Chem.* **71**(24)9381–9390 <https://doi.org/10.1021/acs.jafc.3c00953>(2023).
93. Liu, Y. Q., Ma, Y. Y. & Bi, X. Y. M. Stem Cells Attenuated Blood-Brain Barrier Disruption via Downregulation of Aquaporin-4 Expression in EAE Mice.*Mol Neurobiol.***57**(9),3891–3901.<https://doi.org/10.1007/s12035-020-01998-z>(2020).
94. Chandrakesan, P. et al. S.Novel changes in NF- $\{\kappa\}$ B activity during progression and regression phases of hyperplasia: role of MEK, ERK, and p38. *J. Biol. Chem.* **285** (43), 33485–33498. <https://doi.org/10.1074/jbc.M110.129353> (2010).
95. Li, Y. L. et al. Y.6-Gingerol protects intestinal barrier from ischemia/reperfusion-induced damage via Inhibition of p38 MAPK to NF- κ B signalling. *Pharmacol. Res.* **119**,137–148 <https://doi.org/10.1016/j.phrs.2017.01.026>(2017).
96. Wang, B. F., Cui, Z. W., Sun, H., Yang, Q. E. & Bian Sun,Y,G,Y.L.G.Curcumin attenuates brain edema in mice with intracerebral hemorrhage through Inhibition of AQP4 and AQP9 expression. *Acta Pharmacol. Sin* **36**(8)939–948 <https://doi.org/10.1038/aps.2015.47>(2015).
97. M,T.,T,A.,B,S.,Ak, G. & Sks S.Curcumin prophylaxis refurbishes alveolar epithelial barrier integrity and alveolar fluid clearance under hypoxia. *Respir Physiol. Neurobiol.* **274**, 10336. <https://doi.org/10.1016/j.resp.2019.103336> (2020).
98. Zhao, F. et al. Y.W.Aquapor-in-4 deletion ameliorates hypoglycemia-induced BBB permeability by inhibiting inflammatory responses. *J. Neuroinflammation* **15**(1).<https://doi.org/10.1186/s12974-018-1203-8>(2018).
99. Kanehisa, M. & Goto, S. K. E. G. Kyoto encyclopedia of genes and genomes. *Nucleic Acids Res.* **28**, 27–30. <https://doi.org/10.1093/nar/28.1.27> (2000).
100. Kanehisa, M. Toward Understanding the origin and evolution of cellular organisms.protein sci.**28**, 1947–1951 (2019). <https://doi.org/10.1002/pro.3715>
101. Kanehisa, M., Furumichi, M., Sato, Y., Kawashima, M. & Ishiguro-Watanabe M.KEGG for taxonomy-based analysis of pathways and genomes. *Nucleic Acids Res.* <https://doi.org/10.1093/nar/gkae963> (2023). .51,D587-D592.
102. Xu, R., Bi, Y. P., Zhang, Y. & Zhao X.Kidney-tonify blood-activating Decoction delays ventricular remodeling in rats with chronic heart failure by regulating gut microbiota and metabolites and p38 mitogen-activated protein kinase/p65 nuclear factor kappa-B/aquaporin-4 signaling pathway. *J. Ethnopharmacol.* <https://doi.org/10.1016/j.jep.2024.118110> (2024).
103. Du, H. Y. et al. & Jie,L.G.Tanshinone IIA suppresses proliferation and inflammatory cytokine production of synovial fibroblasts from rheumatoid arthritis patients induced by TNF- α and attenuates the inflammatory response in AIA mice. *Front. Pharmacol.* **11**,568. <https://doi.org/10.3389/fphar.2020.00568>(2020).
104. Liao, X. Z. et al. &Lin,L.Z.Tanshinone IIA combined with cisplatin synergistically inhibits non-small-cell lung cancer in vitro and in vivo via down-regulating the phosphatidylinositol 3-kinase/Akt signalling pathway. *Phytother Res.* **33** (9), 2298–2309. <https://doi.org/10.1002/ptr.6392> (2019).
105. Qian, J. et al. J.G.Tanshinone IIA promotes IL2- mediated SW480 colorectal cancer cell apoptosis by triggering INF2-related mitochondrial fission and activating the Mst1-Hippo pathway.*Biomed Pharmacother.***108**,1658–1669.<https://doi.org/10.1016/j.biopharma.2018.09.170>(2018).

Acknowledgements

This work was supported by the National Natural Science Foundation of China (82174241,81774157).

Author contributions

Rui Xu: Experiment, Data curation, Formal analysis, Investigation, Methodology, Writing-original draft.Yanping Bi: Data curation, Formal analysis, Investigation, Methodology, Software, Writing-original draft.Yetao Ju: Experiment, Formal analysis, Validation.Wenhai Yin: Experiment, Formal analysis, Validation.Shujun Zhao: Formal analysis, Methodology, Validation.Yan Zhang: Conceptualization, Methodology, Project administration, Supervision, Funding acquisition, Writing-review&editing.Xin Zhao: Conceptualization, Project administration, Supervision, Resources, Writing-review&editing.

Declarations

Competing interests

The authors declare no competing interests.

Consent for publication

Not applicable.

Ethics declarations

All experiments strictly followed NIH guidelines (NIH Pub. No. 85 – 23, revised 1996) and the Chinese government's Guide for Laboratory Animal Care (June 3, 2004). And the study is reported in accordance with ARRIVE guidelines. The study received ethical approval from Liaoning University of Traditional Chinese Medicine's Animal Ethics Committee (Approval No. 21000042022076, dated September 26, 2022).

Additional information

Supplementary Information The online version contains supplementary material available at <https://doi.org/10.1038/s41598-025-01276-9>.

Correspondence and requests for materials should be addressed to Y.Z. or X.Z.

Reprints and permissions information is available at www.nature.com/reprints.

Publisher's note Springer Nature remains neutral with regard to jurisdictional claims in published maps and institutional affiliations.

Open Access This article is licensed under a Creative Commons Attribution-NonCommercial-NoDerivatives 4.0 International License, which permits any non-commercial use, sharing, distribution and reproduction in any medium or format, as long as you give appropriate credit to the original author(s) and the source, provide a link to the Creative Commons licence, and indicate if you modified the licensed material. You do not have permission under this licence to share adapted material derived from this article or parts of it. The images or other third party material in this article are included in the article's Creative Commons licence, unless indicated otherwise in a credit line to the material. If material is not included in the article's Creative Commons licence and your intended use is not permitted by statutory regulation or exceeds the permitted use, you will need to obtain permission directly from the copyright holder. To view a copy of this licence, visit <http://creativecommons.org/licenses/by-nc-nd/4.0/>.

© The Author(s) 2025